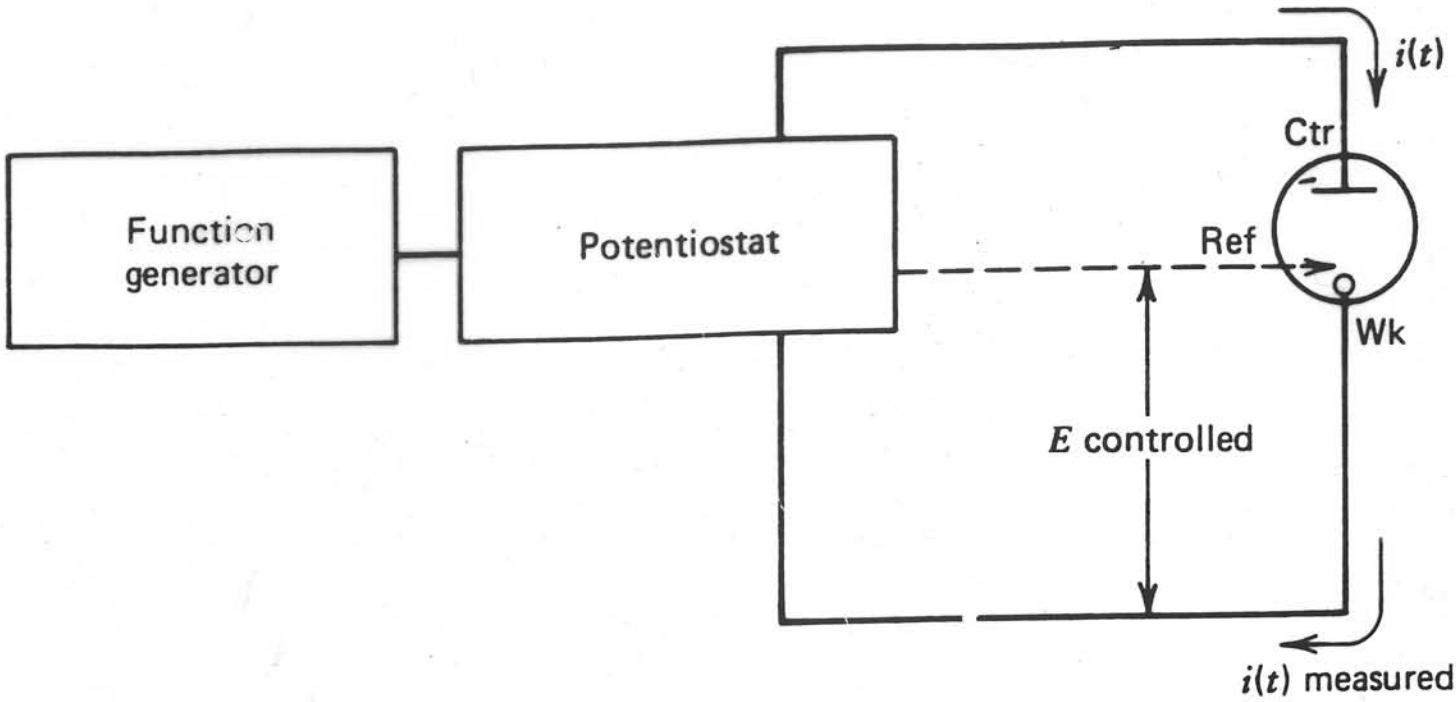

Figure 5.1.1
Schematic experimental arrangement for controlled potential experiments

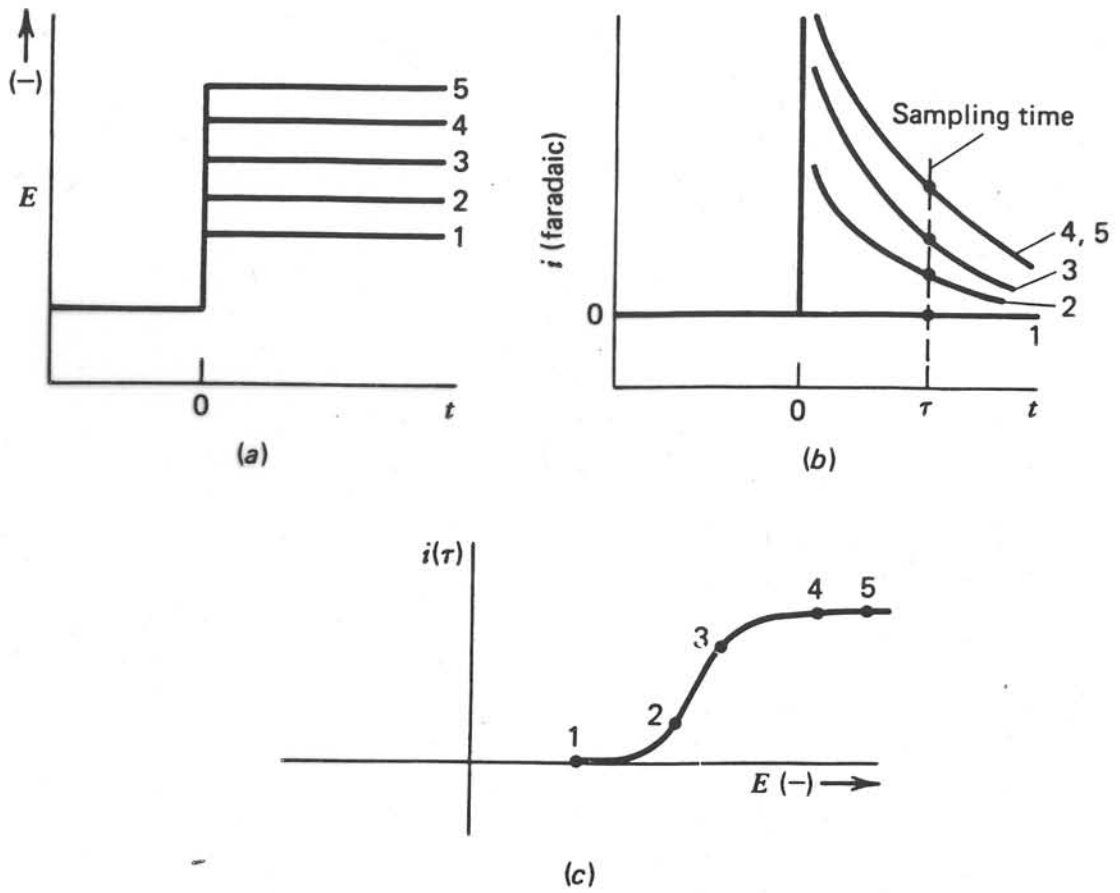

Figure 5.1.3

Sampled-current voltammetry. (*a*) Step waveforms applied in a series of experiments. (*b*) Current-time curves observed in response to the steps. (*c*) Sampled-current voltammogram.

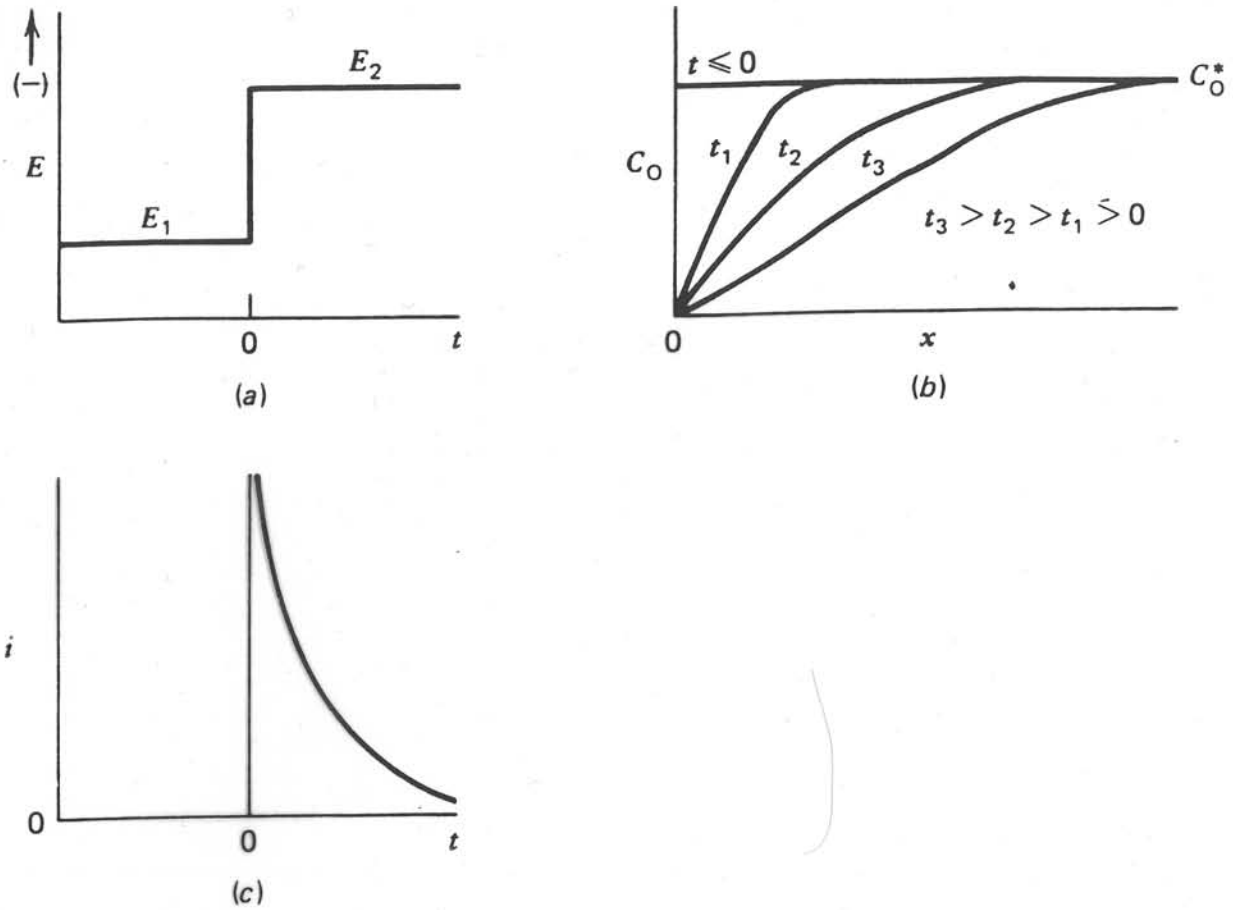

Figure 5.1.2

(*a*) Waveform for a step experiment in which species O is electroinactive at E_1 but is reduced at a diffusion-limited rate at E_2. (*b*) Concentration profiles for various times into the experiment. (*c*) Current flow versus time.

(c) Reversible (Nernstian) Electrode Process

For very rapid electrode kinetics, we have seen that the *i-E* relation collapses generally to a relation of the Nernst form (Sections 3.4.5 and 3.5.3):

$$E = E^{0'} + \frac{RT}{nF} \ln \frac{C_O(0, t)}{C_R(0, t)} \tag{5.1.5}$$

Again the kinetic parameters k^0 and α are not involved, and mathematical treatments are nearly always greatly simplified.

(d) Totally Irreversible Electron Transfer

When the electrode kinetics are very sluggish (k^0 is very small), the anodic and cathodic terms of (5.1.3) are never simultaneously significant. That is, when an appreciable net cathodic current is flowing, the second term in (5.1.3) has a negligibly small effect, and vice versa. To observe the net current, the forward process must be so strongly activated (by application of an overpotential) that the back reaction is virtually totally inhibited. In such cases, observations are always made in the "Tafel region," hence one of the terms in (5.1.3) can be neglected (see also Sections 3.4.3 and 3.5.4).

(e) Quasireversible Systems

Unfortunately, electrode processes are not always facile or very sluggish, and we sometimes must consider the whole *i-E* characteristic. In such *quasireversible* (*or quasi-nernstian* cases), we recognize that the net current involves appreciable activated components from the forward and reverse charge transfers.

In delineating these special situations, we are mostly concentrating on electrode processes that are chemically reversible; however the mechanism of an electrode process often involves an irreversible chemical transformation, such as the decay of the electron-transfer product by a following homogeneous reaction. A good specific example features anthracene in DMF, which we have already considered previously. If a proton donor, such as water, is present in the solvent, the anthracene anion radical is protonated irreversibly and several other steps follow, eventually yielding 9,10-dihydroanthracene. Treating any case in which irreversible chemical steps are linked to heterogeneous electron transfer is much more complicated than dealing with the heterogeneous electron transfer alone. One of the simplified cases, given in (a)–(d) earlier might apply to the electron-transfer step, but the homogeneous kinetics must also be added into the picture. Even in the absence of coupled-solution chemistry, chemically reversible electrode processes can be complicated by multistep heterogeneous electron transfer to a single species. For example, the two-electron reduction of Sn^{4+} to Sn^{2+} can be treated and understood as a sequence of one-electron transfers. In Chapter 12, we will see how more complicated electrode reactions like these can be handled.

▶ 5.2 POTENTIAL STEP UNDER DIFFUSION CONTROL

5.2.1 A Planar Electrode

Previously, we considered an experiment involving an instantaneous change in potential from a value where no electrolysis occurs to a value in the mass-transfer-controlled region for reduction of anthracene, and we were able to grasp the current-time response qualitatively. Here we will develop a quantitative treatment of such an experiment. A planar electrode (e.g., a platinum disk) and an unstirred solution are presumed. In place of the

anthracene example, we can consider the general reaction O + $ne \rightarrow$ R. Regardless of whether the kinetics of this process are basically facile or sluggish, they can be activated by a sufficiently negative potential (unless the solvent or supporting electrolyte is reduced first), so that the surface concentration of O becomes effectively zero. This condition will then hold at any more extreme potential. We will consider our instantaneous step to terminate in this region.

(a) Solution of the Diffusion Equation

The calculation of the diffusion-limited current, i_d, and the concentration profile, $C_O(x, t)$, involves the solution of the linear diffusion equation:

$$\frac{\partial C_O(x, t)}{\partial t} = D_O \frac{\partial^2 C_O(x, t)}{\partial x^2} \tag{5.2.1}$$

under the boundary conditions:

$$C_O(x, 0) = C_O^* \tag{5.2.2}$$

$$\lim_{x \to \infty} C_O(x, t) = C_O^* \tag{5.2.3}$$

$$C_O(0, t) = 0 \quad (\text{for } t > 0) \tag{5.2.4}$$

The *initial condition*, (5.2.2), merely expresses the homogeneity of the solution before the experiment starts at $t = 0$, and the *semi-infinite condition*, (5.2.3), is an assertion that regions distant from the electrode are unperturbed by the experiment. The third condition, (5.2.4), expresses the condition at the electrode surface after the potential transition, and it embodies the particular experiment we have at hand.

Section A.1.6 demonstrates that after Laplace transformation of (5.2.1), the application of conditions (5.2.2) and (5.2.3) yields

$$\bar{C}_O(x, s) = \frac{C_O^*}{s} + A(s)\, e^{-\sqrt{s/D_O}x} \tag{5.2.5}$$

By applying the third condition, (5.2.4), the function $A(s)$ can be evaluated, and then $\bar{C}_O(x, s)$ can be inverted to obtain the concentration profile for species O. Transforming (5.2.4) gives

$$\bar{C}_O(0, s) = 0 \tag{5.2.6}$$

which implies that

$$\bar{C}_O(x, s) = \frac{C_O^*}{s} - \frac{C_O^*}{s} e^{-\sqrt{s/D_O}x} \tag{5.2.7}$$

In Chapter 4, we saw that the flux at the electrode surface is proportional to the current; specifically,

$$-J_O(0, t) = \frac{i(t)}{nFA} = D_O \left[\frac{\partial C_O(x, t)}{\partial x}\right]_{x=0} \tag{5.2.8}$$

which is transformed to

$$\frac{\bar{i}(s)}{nFA} = D_O \left[\frac{\partial \bar{C}_O(x, s)}{\partial x}\right]_{x=0} \tag{5.2.9}$$

The derivative in (5.2.9) can be evaluated from (5.2.7). Substitution yields

$$\bar{i}(s) = \frac{nFAD_O^{1/2} C_O^*}{s^{1/2}} \tag{5.2.10}$$

and inversion produces the current-time response

$$i(t) = i_d(t) = \frac{nFAD_O^{1/2}C_O^*}{\pi^{1/2}t^{1/2}} \tag{5.2.11}$$

which is known as the *Cottrell equation* (3). Its validity was verified in detail by the classic experiments of Kolthoff and Laitinen, who measured or controlled all parameters (1, 2). Note that the effect of depleting the electroactive species near the surface leads to an inverse $t^{1/2}$ function. We will encounter this kind of time dependence frequently in other kinds of experiments. It is a mark of diffusive control over the rate of electrolysis.

In practical measurements of the *i-t* behavior under "Cottrell conditions" one must be aware of instrumental and experimental limitations:

1. *Potentiostatic limitations.* Equation 5.2.11 predicts very high currents at short times, but the actual maximum current may depend on the current and voltage output characteristics of the potentiostat (Chapter 15).
2. *Limitations in the recording device.* During the initial part of the current transient, the oscilloscope, transient recorder, or other recording device may be overdriven, and some time may be required for recovery, after which accurate readings can be displayed.
3. *Limitations imposed by R_u and C_d.* As shown in Section 1.2.4, a nonfaradaic current must also flow during a potential step. This current decays exponentially with a *cell time constant*, R_uC_d (where R_u is the uncompensated resistance and C_d is the double-layer capacitance). For a period of about five time constants, an appreciable contribution of charging current to the total measured current exists, and this superimposed signal can make it difficult to identify the faradaic current precisely. Actually, the charging of the double layer is the mechanism that establishes a change in potential; hence the cell time constant also defines the shortest time scale for carrying out a step experiment. The time during which data are collected after a step is applied must be much greater than R_uC_d if an experiment is to fulfill the assumption of a practically instantaneous change in surface concentration at $t = 0$ (see Sections 1.2.4 and 5.9.1).
4. *Limitations due to convection.* At longer times the buildup of density gradients and stray vibrations will cause convective disruption of the diffusion layer, and usually result in currents larger than those predicted by the Cottrell equation. The time for the onset of convective interference depends on the orientation of the electrode, the existence of a protective mantle around the electrode, and other factors (1, 2). In water and other fluid solvents, diffusion-based measurements for times longer than 300 s are difficult, and even measurements longer than 20 s may show some convective effects.

(b) Concentration Profile

Inversion of (5.2.7) yields

$$C_O(x, t) = C_O^*\left\{1 - \text{erfc}\left[\frac{x}{2(D_Ot)^{1/2}}\right]\right\} \tag{5.2.12}$$

or

$$C_O(x, t) = C_O^* \,\text{erf}\left[\frac{x}{2(D_Ot)^{1/2}}\right] \tag{5.2.13}$$

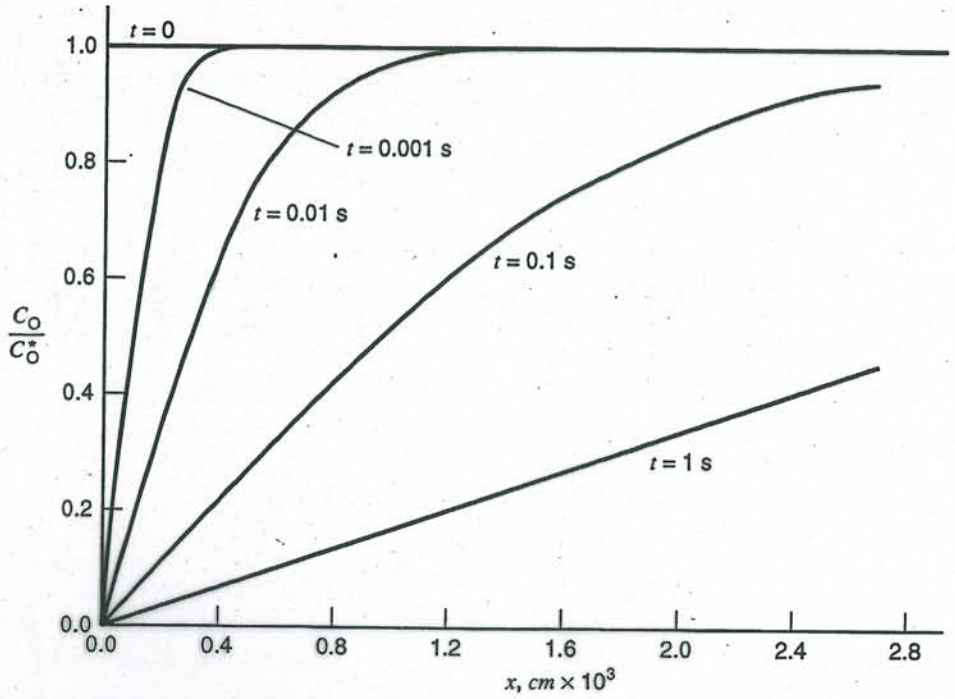

Figure 5.2.1 Concentration profiles for several times after the start of a Cottrell experiment. $D_O = 1 \times 10^{-5}$ cm^2/s.

Figure 5.2.1 comprises several plots from (5.2.13) for various values of time. The depletion of O near the electrode is easily seen, as is the time-dependent falloff in the concentration gradient at the electrode surface, which leads to the monotonically decreasing i_d function of (5.2.11).

One can also see from Figure 5.2.1 that the *diffusion layer*, that is the zone near the electrode where concentrations differ from those of the bulk, has no definite thickness. The concentration profiles asymptotically approach their bulk values. Still, it is useful to think about the thickness in terms of $(D_O t)^{1/2}$, which has units of length and characterizes the distance that species O can diffuse in time t. Note that the argument of the error function in (5.2.13) is the distance from the electrode expressed in units of $2(D_O t)^{1/2}$. The error function rises very rapidly toward its asymptote of 1 (see Section A.3). When its arguments are 1, 2, and 3 (i.e., when x is 2, 4, and 6 times $(D_O t)^{1/2}$), it has values, respectively, of 0.84, 0.995, and 0.99998; thus the diffusion layer is completely contained within a distance of $6(D_O t)^{1/2}$ from the electrode. For most purposes, one can think of it as being somewhat thinner. People often talk of a *diffusion layer thickness*, because there is a need to describe the reach of the electrode process into the solution. At distances much greater than the diffusion layer thickness, the electrode can have no appreciable effect on concentrations, and the reactant molecules there have no access to the electrode. At distances much smaller, the electrode process is powerfully dominant. Even though no consistent or accepted definition exists, people often define the thickness as 1, $2^{1/2}$, $\pi^{1/2}$, or 2 times $(D_O t)^{1/2}$. Any of these ideas suffices. We have already seen diffusion lengths defined in different ways in Sections 1.4.3 and 4.4.1.

Of course the thickness of the diffusion layer depends significantly on the time scale of the experiment, as one can see in Figure 5.2.1. For a species with a diffusion coefficient of 1×10^{-5} cm^2 s^{-1}, $(D_O t)^{1/2}$ is about 30 μm for an experimental time of 1 s, but only 1 μm at 1 ms, and just 30 nm at 1 μs.

5.2.2 Semi-Infinite Spherical Diffusion

If the electrode in the step experiment is spherical rather than planar (e.g., a hanging mercury drop), one must consider a spherical diffusion field, and Fick's second law becomes

$$\frac{\partial C_O(r,t)}{\partial t} = D_O\left\{\frac{\partial^2 C_O(r,t)}{\partial r^2} + \frac{2}{r}\frac{\partial C_O(r,t)}{\partial r}\right\} \tag{5.2.14}$$

where r is the radial distance from the electrode center. The boundary conditions are then

$$C_O(r,0) = C_O^* \quad (r > r_0) \tag{5.2.15}$$

$$\lim_{r\to\infty} C_O(r,t) = C_O^* \tag{5.2.16}$$

$$C_O(r_0,t) = 0 \quad (t > 0) \tag{5.2.17}$$

where r_0 is the radius of the electrode.

(a) Solution of the Diffusion Equation

The substitution, $v(r,t) = rC_O(r,t)$, converts (5.2.14) into an equation having the same form as the linear problem. The details are left to the reader (Problem 5.1). The resulting diffusion current is

$$\boxed{i_d(t) = nFAD_OC_O^*\left[\frac{1}{(\pi D_O t)^{1/2}} + \frac{1}{r_0}\right]} \tag{5.2.18}$$

which can be written

$$i_d(\text{spherical}) = i_d(\text{linear}) + \frac{nFAD_OC_O^*}{r_0} \tag{5.2.19}$$

Thus the diffusion current for the spherical case is just that for the linear situation plus a constant term. For a planar electrode,

$$\lim_{t\to\infty} i_d = 0 \tag{5.2.20}$$

but in the spherical case,

$$\lim_{t\to\infty} i_d = \frac{nFAD_OC_O^*}{r_0} \tag{5.2.21}$$

The reason for this curious nonzero limit is that one converges on a situation in which the growth of the depletion region fails to affect the concentration gradients at the surface because the diffusion field is able to draw material from a continually larger area at its outer limit. In actual experiments with working electrodes of millimeter diameters or larger, convection caused by density gradients or vibration becomes important at longer times and enhances the mass transfer, so that the diffusive steady state is rarely reached. On the other hand, it is easy to reach this condition with UMEs (radius of 25 μm or smaller), and the ability to exploit the steady state is one of their principal advantages (see Section 5.3).

(b) Concentration Profile

The distribution of the electroactive species near the electrode also can be obtained from the solution to the diffusion equation, and it turns out to be

$$C_O(r,t) = C_O^*\left[1 - \frac{r_0}{r}\operatorname{erfc}\left(\frac{r-r_0}{2(D_Ot)^{1/2}}\right)\right] \tag{5.2.22}$$

Because $r - r_0$ is the distance from the electrode surface, this profile strongly resembles that for the linear case (equation 5.2.12). The difference is the factor r_0/r and, if the diffusion layer is thin compared to the electrode's radius, the linear and spherical cases are indistinguishable. The situation is directly analogous to our experience in living on a spherical planet. The zone of our activities above the earth's surface is small compared to its radius of curvature; hence we usually cannot distinguish the surface from a rough plane.

At the other extreme, when the diffusion layer grows much larger than r_0 (as at a UME), the concentration profile near the surface becomes independent of time and linear with $1/r$. One can see this effect in (5.2.22), where error function complement approaches unity for $(r - r_0) << 2(D_O t)^{1/2}$. In that case,

$$C_O(r, t) = C_O^*(1 - r_0/r) \tag{5.2.23}$$

The slope at the surface is C_O^*/r_0, which gives the steady-state current, (5.2.21), from the current-flux relationship for the spherical case,

$$\frac{i}{nFA} = D_O\left[\frac{\partial C_O(r, t)}{\partial r}\right]_{r=r_0} \tag{5.2.24}$$

(c) Applicability of the Linear Approximation

These ideas indicate that linear diffusion adequately describes mass transport to a sphere, provided the sphere's radius is large enough and the time domain of interest is small enough. More precisely, the linear treatment is adequate as long as the second (constant) term of (5.2.18) is small compared to the Cottrell term. For accuracy within $a\%$,

$$\frac{nFAD_O C_O^*}{r_0} \leq \frac{a}{100} \cdot \frac{nFAD_O^{1/2} C_O^*}{(\pi t)^{1/2}} \tag{5.2.25}$$

or

$$\frac{\pi^{1/2} D_O^{1/2} t^{1/2}}{r_0} \leq \frac{a}{100} \tag{5.2.26}$$

With $a = 10\%$ and $D_O = 10^{-5}$ cm^2/s, $t^{1/2}/r_0 \leq 18$ s$^{1/2}$/cm. A typical mercury drop might be 0.1 cm in radius; hence the linear treatment holds within 10% for about 3 s.

The numerator of (5.2.26) is the thickness of the diffusion layer; thus the importance of the steady-state term, which manifests spherical diffusion, depends mainly on the ratio of that thickness to the radius of the electrode. When the diffusion layer grows to a thickness that is an appreciable fraction of r_0, it is no longer appropriate to use equations for linear diffusion, and one can expect the steady-state term to contribute significantly to the measured current.

5.2.3 Microscopic and Geometric Areas

If the electrode surface is strictly a plane with a well-defined boundary, such as an atomically smooth metal disk mounted in a glass mantle, the area A in the Cottrell equation is easily understood. On the other hand, real electrode surfaces are not smooth planes, and the concept of area becomes much less clear. Figure 5.2.2 helps to define two different measures of area for a given electrode. First there is the *microscopic area*, which is computed by integrating the exposed surface over all of its undulations, crevices, and asperities, even down to the atomic level. An easier quantity to evaluate operationally, is the *geometric area* (sometimes called the *projected area*). Mathemati-

TABLE 5.3.1 Form of m_O for UMEs of Different Geometries

Band[a]	Cylinder[a]	Disk	Hemisphere	Sphere
$\frac{2\pi D_O}{w\ln(64D_Ot/w^2)}$	$\frac{2D_O}{r_O \ln \tau}$	$\frac{4D_O}{\pi r_O}$	$\frac{D_O}{r_O}$	$\frac{D_O}{r_O}$

[a] Long-time limit is to a quasi-steady state.

5.3.3 Summary of Behavior at Ultramicroelectrodes

Although there are some important differences in the behavior of UMEs with different shapes, it is useful here to recollect some common features in the responses to a large-amplitude potential step:

First, at short times, where the diffusion-layer thickness is small compared to the critical dimension, the current at any UME follows the Cottrell equation, (5.2.11), and semi-infinite linear diffusion applies.

Second, at long times, where the diffusion-layer thickness is large compared to the critical dimension, the current at any UME approaches a steady state or a quasi-steady state. One can write the current in this limit in the manner developed empirically in Section 1.4.2,

$$i_{ss} = nFAm_OC_O^* \tag{5.3.16}$$

where m_O is a mass-transfer coefficient. The functional form of m_O depends on geometry as given in Table 5.3.1.

In practical experiments with UMEs, one normally tries to control the experimental conditions so that the electrode is operating either in the short-time regime (called the *early transient regime* or the *regime of semi-infinite linear diffusion* in the remainder of this book) or in the long-time limit (called the *steady-state regime*). The transition region between these two limiting regimes involves much more complicated theory and offers no advantage, so we will not be considering it in much detail.

▶ 5.4 SAMPLED-CURRENT VOLTAMMETRY FOR REVERSIBLE ELECTRODE REACTIONS

The basic experimental methodology for sampled-current voltammetry is described in Section 5.1.1, especially in the text surrounding Figure 5.1.3. After studying the diffusion-controlled responses to potential steps in Sections 5.2 and 5.3, we now understand that the result of a sampled-current experiment might depend on whether the sampling occurs in the time regime where a transient current flows or in the later period, when a steady-state could be reached. This idea leads us to consider the two modes separately for reversible chemistry in Sections 5.4.1 and 5.4.2 below. Applications of reversible voltammograms are then treated in Section 5.4.4.

5.4.1 Voltammetry Based on Linear Diffusion at a Planar Electrode

(a) A Step to an Arbitrary Potential

Consider again the reaction $O + ne \rightleftarrows R$ in a Cottrell-like experiment at an electrode where semi-infinite linear diffusion applies,[5] but this time let us treat potential steps of

[5] It is most natural to think of this experiment as taking place at a planar electrode, but as shown in Sections 5.2.2 and 5.3, the required condition is realized with any electrode shape as long as the diffusion layer thickness remains small compared to the radius of curvature of the electrode.

any magnitude. We begin each experiment at a potential at which no current flows; and at $t = 0$, we change E instantaneously to a value anywhere on the reduction wave. We assume here that charge-transfer kinetics are very rapid, so that

$$E = E^{0'} + \frac{RT}{nF} \ln \frac{C_O(0, t)}{C_R(0, t)} \tag{5.4.1}$$

always.

The equations governing this case are[6]

$$\frac{\partial C_O(x, t)}{\partial t} = D_O \frac{\partial^2 C_O(x, t)}{\partial x^2} \qquad \frac{\partial C_R(x, t)}{\partial t} = D_R \frac{\partial^2 C_R(x, t)}{\partial x^2} \tag{5.4.2}$$

$$C_O(x, 0) = C_O^* \qquad C_R(x, 0) = 0 \tag{5.4.3}$$

$$\lim_{x \to \infty} C_O(x, t) = C_O^* \qquad \lim_{x \to \infty} C_R(x, t) = 0 \tag{5.4.4}$$

and the flux balance is

$$D_O \left(\frac{\partial C_O(x, t)}{\partial x} \right)_{x=0} + D_R \left(\frac{\partial C_R(x, t)}{\partial x} \right)_{x=0} = 0 \tag{5.4.5}$$

It is convenient to rewrite (5.4.1) as

$$\theta = \frac{C_O(0, t)}{C_R(0, t)} = \exp\left[\frac{nF}{RT} (E - E^{0'}) \right] \tag{5.4.6}$$

In Section 5.2.1, we saw that application of the Laplace transform to (5.4.2) and consideration of conditions (5.4.3) and (5.4.4) would yield

$$\bar{C}_O(x, s) = \frac{C_O^*}{s} + A(s)\, e^{-\sqrt{s/D_O}x} \tag{5.4.7}$$

$$\bar{C}_R(x, s) = B(s)\, e^{-\sqrt{s/D_R}x} \tag{5.4.8}$$

Transformation of (5.4.5) gives

$$D_O \left(\frac{\partial \bar{C}_O(x, s)}{\partial x} \right)_{x=0} + D_R \left(\frac{\partial \bar{C}_R(x, s)}{\partial x} \right)_{x=0} = 0 \tag{5.4.9}$$

which can be simplified by evaluating the derivatives from (5.4.7) and (5.4.8):

$$-A(s)\, D_O^{1/2}\, s^{1/2} - B(s)\, D_R^{1/2}\, s^{1/2} = 0 \tag{5.4.10}$$

Thus, $B = -A(s)\xi$, where $\xi = (D_O/D_R)^{1/2}$. So far we have not invoked the Nernst relation, (5.4.1); hence our results:

$$\bar{C}_O(x, s) = \frac{C_O^*}{s} + A(s)\, e^{-(s/D_O)^{1/2}x} \tag{5.4.11}$$

$$\bar{C}_R(x, s) = -A(s)\xi\, e^{-(s/D_R)^{1/2}x} \tag{5.4.12}$$

hold for any i-E characteristic. We will make use of this fact in Section 5.5.

We introduce the assumption of reversibility to evaluate $A(s)$. Transformation of (5.4.6) shows that $\bar{C}_O(0, s) = \theta \bar{C}_R(0, s)$; thus

$$\frac{C_O^*}{s} + A(s) = -\xi\theta A(s) \tag{5.4.13}$$

[6]Clearly, (5.4.3) implies that R is initially absent. The case for $C_R(x, 0) = C_R^*$, follows analogously, and is left as Problem 5.10.

and $A(s) = -\bar{C}_O^*/s(1 + \xi\theta)$. The transformed profiles are then

$$\bar{C}_O(x, s) = \frac{C_O^*}{s} - \frac{C_O^* e^{-(s/D_O)^{1/2}x}}{s(1 + \xi\theta)} \tag{5.4.14}$$

$$\bar{C}_R(x, s) = \frac{\xi C_O^* e^{-(s/D_R)^{1/2}x}}{s(1 + \xi\theta)} \tag{5.4.15}$$

Equation 5.4.14 differs from (5.2.7) only by the factor $1/(1 + \xi\theta)$ in the second term. Since $(1 + \xi\theta)$ is independent of x and t, the current can be obtained exactly as in the treatment of the Cottrell experiment by evaluating $\bar{i}(s)$ and then inverting:

$$i(t) = \frac{nFAD_O^{1/2}C_O^*}{\pi^{1/2}\, t^{1/2}\, (1 + \xi\theta)} \tag{5.4.16}$$

This relation is the general response function for a step experiment in a reversible system. The Cottrell equation, (5.2.11), is a special case for the diffusion-limited region, which requires a very negative $E - E^{0'}$, so that $\theta \to 0$. It is convenient to represent the Cottrell current as $i_d(t)$ and to rewrite (5.4.16) as

$$i(t) = \frac{i_d(t)}{1 + \xi\theta} \tag{5.4.17}$$

Cottrell current

Scale factor

Now we see that for a reversible couple, every current-time curve has the same shape; but its magnitude is scaled by $1/(1 + \xi\theta)$ according to the potential to which the step is made. For very positive potentials (relative to $E^{0'}$), this scale factor is zero; thus $i(t)$ has a value between zero and $i_d(t)$, depending on E, as sketched in Figure 5.1.3.

(b) Shape of the Current-Potential Curve i-E characteristic

In sampled-current voltammetry, our goal is to obtain an $i(\tau)$-E curve by (a) performing several step experiments with different final potentials E, (b) sampling the current response at a fixed time τ after the step, and (c) plotting $i(\tau)$ *vs.* E. Here we consider the shape of this curve for a reversible couple and the kinds of information one can obtain from it.

Equation 5.4.17 really answers the question for us. For a fixed sampling time τ,

$$i(\tau) = \frac{i_d(\tau)}{1 + \xi\theta} \tag{5.4.18}$$

which can be rewritten as

$$\xi\theta = \frac{i_d(\tau) - i(\tau)}{i(\tau)} \tag{5.4.19}$$

and expanded:

i-E implicit

$$E = E^{0'} + \frac{RT}{nF} \ln \frac{D_R^{1/2}}{D_O^{1/2}} + \frac{RT}{nF} \ln \frac{i_d(\tau) - i(\tau)}{i(\tau)} \tag{5.4.20}$$

When $i(\tau) = i_d(\tau)/2$, the current ratio becomes unity so that the third term vanishes. The potential for which this is so is $E_{1/2}$, the *half-wave potential*:

$$E_{1/2} = E^{0'} + \frac{RT}{nF} \ln \frac{D_R^{1/2}}{D_O^{1/2}} \tag{5.4.21}$$

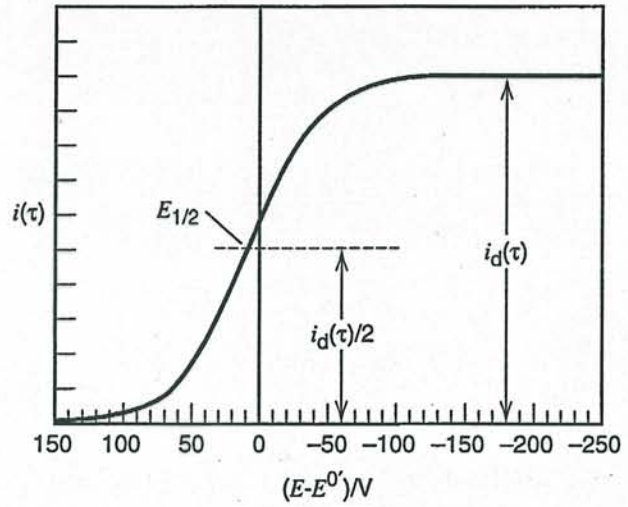

Figure 5.4.1 Characteristics of a reversible wave in sampled-current voltammetry. This curve is for $n = 1$, $T = 298$ K, and $D_O = D_R/2$. Because $D_O \neq D_R$, $E_{1/2}$ differs slightly from $E^{0'}$, in this case by about 9 mV. For $n > 1$, the wave rises more sharply to the plateau (see Figure 5.4.2).

and (5.4.20) is often written

$$E = E_{1/2} + \frac{RT}{nF} \ln \frac{i_d(\tau) - i(\tau)}{i(\tau)} \tag{5.4.22}$$

These equations describe the voltammogram for a reversible system in sampled-current voltammetry as long as semi-infinite linear diffusion holds. It is interesting to compare (5.4.20) and (5.4.22) with the wave shape equations derived in a naive way for steady-state voltammetry in Section 1.4.2(a). They are identical in form.

As shown in Figure 5.4.1, these relations predict a wave that rises from baseline to the diffusion-controlled limit over a fairly narrow potential region (~200 mV) centered on $E_{1/2}$. Since the ratio of diffusion coefficients in (5.4.21) is nearly unity in almost any case, $E_{1/2}$ is usually a very good approximation to $E^{0'}$ for a reversible couple.

Note also that E *vs.* log $[(i_d - i)/i]$ should be linear with a slope of $2.303RT/nF$ or $59.1/n$ mV at 25°C. This "wave slope" is often computed for experimental data to test for reversibility. A quicker test [the *Tomeš criterion* (25)] is that $|E_{3/4} - E_{1/4}| = 56.4/n$ mV at 25°C. The potentials $E_{3/4}$ and $E_{1/4}$ are those for which $i = 3i_d/4$ and $i = i_d/4$, respectively. If the wave slope or the Tomeš criterion significantly exceeds the expected values, the system is not reversible. (See also Section 5.5.4).

(c) Concentration Profiles

Taking the inverse transforms of (5.4.14) and (5.4.15) yields the concentration profiles:

$$C_O(x, t) = C_O^* - \frac{C_O^*}{1 + \xi\theta} \operatorname{erfc}\left[\frac{x}{2(D_O t)^{1/2}}\right] \tag{5.4.23}$$

$$C_R(x, t) = \frac{\xi C_O^*}{1 + \xi\theta} \operatorname{erfc}\left[\frac{x}{2(D_R t)^{1/2}}\right] \tag{5.4.24}$$

Some other convenient equations relating to concentrations can also be written. Let us solve for $A(s)$ and $B(s)$ in (5.4.7) and (5.4.8) in terms of the transformed surface concentrations $\bar{C}_O(0, s)$, and $\bar{C}_R(0, s)$, then substitute into (5.4.10):

$$D_O^{1/2}\left(\bar{C}_O(0, s) - \frac{C_O^*}{s}\right) + D_O^{1/2}\bar{C}_R(0, s) = 0 \tag{5.4.25}$$

or, using the inverse transform,

$$D_O^{1/2} C_O(0, t) + D_R^{1/2} C_R(0, t) = C_O^* D_O^{1/2} \tag{5.4.26}$$

The more general relation for R initially present is

$$D_O^{1/2}C_O(0,t) + D_R^{1/2}C_R(0,t) = C_O^* D_O^{1/2} + C_R^* D_R^{1/2} \tag{5.4.27}$$

For the special case when $D_O = D_R$,

$$C_O(0,t) + C_R(0,t) = C_O^* + C_R^* \tag{5.4.28}$$

Equations 5.4.26 to 5.4.28 were derived without reference to the sixth boundary condition in the diffusion problem; hence they do not depend on any particular electrochemical perturbation or *i-E* function, and they hold for virtually any electrochemical method. The principal assumptions are that semi-infinite linear diffusion applies and that O and R are soluble, stable species.[7]

Returning now to the step experiments for which (5.4.23) and (5.4.24) apply, we see that the surface concentrations are

$$C_O(0,t) = C_O^*\left(1 - \frac{1}{1+\xi\theta}\right) = C_O^*\left(\frac{\xi\theta}{1+\xi\theta}\right) \tag{5.4.29}$$

$$C_R(0,t) = C_O^*\left(\frac{\xi}{1+\xi\theta}\right) \tag{5.4.30}$$

Since (5.4.17) shows that $i(t)/i_d(t) = 1/(1+\xi\theta)$,

$$C_O(0,t) = C_O^*\left[1 - \frac{i(t)}{i_d(t)}\right] \tag{5.4.31}$$

$$C_R(0,t) = \xi C_O^* \frac{i(t)}{i_d(t)} \tag{5.4.32}$$

We will use these relations in Section 5.4.3 to simplify the interpretation of reversible sampled-current voltammograms in various chemical situations. The reader interested in a quick view of applications can proceed directly to that point and beyond. However, a full view of reversible waves needs to include those recorded by sampling steady-state currents, so the next section is devoted to that topic.

5.4.2 Steady-State Voltammetry at a UME

(a) A Step to an Arbitrary Potential at a Spherical Electrode

Let us consider again the reaction $O + ne \rightleftarrows R$ in an experiment involving a step of any magnitude, but in contrast to the limitations of the previous section, let us allow the experiment to proceed beyond the regime where semi-infinite linear diffusion applies. For the moment let us also restrict the electrode geometry to a sphere or hemisphere of radius r_0. Species O is present in the bulk, but R is absent. We begin each experiment at a potential at which no current flows; and at $t = 0$, we change E instantaneously to a value anywhere on the reduction wave.

The governing equations are

$$\frac{\partial C_O(r,t)}{\partial t} = D_O\left(\frac{\partial^2 C_O(r,t)}{\partial r^2} + \frac{2}{r}\frac{\partial C_O(r,t)}{\partial r}\right) \tag{5.4.33}$$

[7]Note also that for the step experiments under discussion, (5.4.23) and (5.4.24) show that $C_O(x,t) + C_R(x,t) = C_O^*$ at any point along the profiles, when $D_O = D_R$.

5.4.3 Simplified Current-Concentration Relationships

Our treatments of sampling in both the early transient regime and the steady-state regime produced simple linkages between the surface concentrations and the current. For the early transient regime, the relationships (5.4.31) and (5.4.32) can be rearranged and re-expressed by recognizing i_d as the Cottrell relation:

$$i(t) = \frac{nFAD_O^{1/2}}{\pi^{1/2}t^{1/2}}[C_O^* - C_O(0,t)] \tag{5.4.65}$$

$$i(t) = \frac{nFAD_R^{1/2}}{\pi^{1/2}t^{1/2}}C_R(0,t) \tag{5.4.66}$$

Since these relations hold at any time along the current decay, for sampled voltammetry we can replace t by the sampling time τ. Likewise, for the steady-state regime at a sphere, equations (5.4.63) and (5.4.64) can be rearranged and reexpressed as

$$i = \frac{nFAD_O}{r_0}[C_O^* - C_O(0,t)] \tag{5.4.67}$$

$$i = \frac{nFAD_R}{r_0}C_R(0,t) \tag{5.4.68}$$

where the distance variable r has been converted to $r - r_0$ in the interest of comparability with (5.4.65) and (5.4.66) and related equations elsewhere in the book.

For either sampling regime, we arrive with rigor at a set of simple relations of precisely the same form as those *assumed* in the naive approach to mass transport used in Section 1.4. When early transients are sampled, one need only replace m_O with $D_O{}^{1/2}/\pi^{1/2}t^{1/2}$ and m_R with $D_R{}^{1/2}/\pi^{1/2}t^{1/2}$ to translate the relationships exactly. For sampled-current voltammetry under steady-state conditions at a sphere or hemisphere, one instead identifies m_O with D_O/r_0 and m_R with D_R/r_0. Similarly, m_O and m_R for steady state at a disk UME are $(4/\pi)D_O/r_0$ and $(4/\pi)D_R/r_0$, respectively (Table 5.3.1). The two approaches to deriving the i-E curve can be compared as follows:

Naive Approach

Nernstian behavior and $i = nFAm_O[C_O^* - C_O(0,t)]$ $i = nFAm_R[C_R(0,t) - C_R^*]$ were assumed $\xrightarrow[\text{math}]{\text{Simple}}$ i-E curve

Rigorous Approach

Nernstian behavior, diffusion equations, and boundary conditions were assumed $\xrightarrow[\text{math}]{\text{More complex}}$ i-E curve as before and $i = nFAm_O[C_O^* - C_O(0,t)]$ $i = nFAm_R[C_R(0,t) - C_R^*]$ also as before

The rigorous treatment has therefore justified the i-C linkages used before, and it increases confidence in the simpler approach as a means for treating other systems.

The essential reason for the general applicability of these equations is that, in reversible systems, the potential controls the surface concentrations directly and maintains uniformity in these concentrations everywhere on the face of the working electrode. Thus the geometry of the diffusion field, either at steady state or as long as semi-infinite linear diffusion holds, does not depend on potential, and the gradient of that field is simply proportional to the difference between the surface and bulk concentrations.

5.4.4 Applications of Reversible *i-E* Curves

(a) Information from the Wave Height

The plateau current of a simple reversible wave is controlled by mass transfer and can be used to determine any single system parameter that affects the limiting flux of electroreactant at the electrode surface. For waves based on either the sampling of early transients or steady-state currents, the accessible parameters are the n-value of the electrode reaction, the area of the electrode, and the diffusion coefficient and bulk concentration of the electroactive species. Certainly the most common application is to employ wave heights to determine concentrations, typically either by calibration or standard addition. The analytical application of sampled-current voltammetry is discussed more fully in Sections 7.1.3 and 7.3.6.

The plateau currents of steady-state voltammograms can also provide the critical dimension of the electrode (e.g., r_0 for a sphere or disk). When a new UME is constructed, its critical dimension is often not known; however, it can be easily determined from a single voltammogram recorded for a solution of a species with a known concentration and diffusion coefficient, such as $Ru(NH_3)_6^{3+}$ [$D = 5.3 \times 10^{-6}$ cm^2/s in 0.09 M phosphate buffer, pH 7.4 (8)].

(b) Information from the Wave Shape

With respect to the heterogeneous electron-transfer process, reversible (nernstian) systems are always at equilibrium. The kinetics are so facile that the interface is governed solely by thermodynamic aspects. Not surprisingly, then, the shapes and positions of reversible waves, which reflect the energy dependence of the electrode reaction, can be exploited to provide thermodynamic properties, such as standard potentials, free energies of reaction, and various equilibrium constants, just as potentiometric measurements can be. On the other hand, reversible systems can offer no kinetic information, because the kinetics are, in effect, transparent.

The wave shape is most easily analyzed in terms of the "wave slope," which is expected to be $2.303RT/nF$ (i.e., $59.1/n$ mV at 25°C) for a reversible system. Larger slopes are generally found for systems that do not have both nernstian heterogeneous kinetics and overall chemical reversibility [Section 5.5.4(b)]; thus the slope can be used to diagnose reversibility. If the system is known to be reversible, the wave slope can be used alternatively to suggest the value of n. Often one finds the idea that a wave slope near 60 mV can be taken as an indicator of *both* reversibility and an n-value of 1. If the electrode reaction is simple and does not implicate, for example, adsorbed species (Chapter 14), one can accurately draw both conclusions from the wave slope. However, electrode reactions are often subtly complex, and it is safer to determine reversibility by a technique that can view the reaction in both directions, such as cyclic voltammetry (Chapter 6). One can then test the conclusion against the observed wave slope in sampled-current voltammetry, which can also suggest the value of n.

(c) Information from the Wave Position

Because the half-wave potential for a reversible wave is very close to $E^{0'}$, sampled-current voltammetry is readily employed to estimate the formal potentials for chemical systems that have not been previously characterized. It is essential to verify reversibility, because $E_{1/2}$ can otherwise be quite some distance from $E^{0'}$ (see Sections 1.5.2 and 5.5 and Chapter 12).

By definition, a formal potential describes the potential of a couple at equilibrium in a system where the oxidized and reduced forms are present at unit formal concentration,

members of a conjugate acid-base pair). Formal potentials always manifest activity coefficients. Frequently they also reflect chemical effects, such as complexation or participation in acid-base equilibria. Thus the formal potential can shift systematically as the medium changes. In sampled-current voltammetry the half-wave potential of a recorded wave would shift correspondingly. This phenomenon provides a highly profitable route to chemical information and has been exploited elaborately.

As a first example, let us consider the kinds of information that are contained in the sampled-current voltammogram for the reversible reduction of a complex ion, such as $Zn(NH_3)_4^{2+}$ in an aqueous ammonia buffer at a mercury drop electrode,[8]

$$Zn(NH_3)_4^{2+} + 2e + Hg \rightleftarrows Zn(Hg) + 4NH_3 \tag{5.4.69}$$

To treat this problem, we derive the *i-E* curve using the simplified approach, as justified in the preceding sections. For generality, the process is represented as

$$MX_p + ne + Hg \rightleftarrows M(Hg) + pX \tag{5.4.70}$$

where the charges on the metal, M, and the ligands, X, are omitted for simplicity. For $M + ne + Hg \rightleftarrows M(Hg)$,

$$E = E_M^{0'} + \frac{RT}{nF} \ln \frac{C_M(0, t)}{C_{M(Hg)}(0, t)} \tag{5.4.71}$$

and for $M + pX \rightleftarrows MX_p$

$$K_c = \frac{C_{MX_p}}{C_M C_X^p} \tag{5.4.72}$$

The presumption of reversibility implies that both of these processes are simultaneously at equilibrium. Substituting (5.4.72) into (5.4.71), we obtain

$$E = E_M^{0'} - \frac{RT}{nF} \ln K_c - \frac{pRT}{nF} \ln C_X(0, t) + \frac{RT}{nF} \ln \frac{C_{MX_p}(0, t)}{C_{M(Hg)}(0, t)} \tag{5.4.73}$$

Let us now add the assumptions (a) that initially $C_{M(Hg)} = 0$, $C_{MX_p} = C_{MX_p}^*$, and $C_X = C_X^*$ and (b) that $C_X^* >> C_{MX_p}^*$. For the specific example involving the zinc ammine complex, the latter condition would be assured by the strength of the buffer, in which ammonia would typically be present at 100 m*M* to 1 *M*, very much above the concentration of the complex, which would normally be at 1 m*M* or even lower. Even though reduction liberates ammonia and oxidation consumes it, the electrode process cannot have an appreciable effect on the value of C_X at the surface, and $C_X(0, t) \approx C_X^*$. Then the following relations apply:

$$i(t) = nFAm_C[\, C_{MX_p}^* - C_{MX_p}(0, t)] \tag{5.4.74}$$

$$i(t) = nFAm_A C_{M(Hg)}(0, t) \tag{5.4.75}$$

$$i_d(t) = nFAm_C C_{MX_p}^* \tag{5.4.76}$$

or,

$$C_{MX_p}(0, t) = \frac{i_d(t) - i(t)}{nFAm_C} \tag{5.4.77}$$

$$C_{M(Hg)}(0, t) = \frac{i(t)}{nFAm_A} \tag{5.4.78}$$

[8]Zinc deposits in the mercury during the potential steps; thus a question arises about how the initial conditions are restored after each cycle in a sampled-current voltammetric experiment. Because the system is reversible, one can rely on reversed electrolysis at the base potential imposed before each step to restore the initial

Substituting (5.4.77) and (5.4.78) into (5.4.73), we obtain

$$E = E^{C}_{1/2} + \frac{RT}{nF} \ln\left[\frac{i_d(t) - i(t)}{i(t)}\right] \tag{5.4.79}$$

with

$$E^{C}_{1/2} = E^{0'}_{M} - \frac{RT}{nF} \ln K_c - \frac{pRT}{nF} \ln C^{*}_{X} + \frac{RT}{nF} \ln \frac{m_A}{m_C} \tag{5.4.80}$$

It is clear now that the wave *shape* is the same as that for the simple redox process $O + ne \rightleftarrows R$, but the *location* of the wave on the potential axis depends on K_c and C^{*}_{X}, in addition to the formal potential of the metal/amalgam couple. For a given K_c, increased concentrations of the complexing agent shift the wave to more extreme potentials. In the specific chemical example that we have been discussing, the effect of complexation by ammonia is to stabilize Zn(II), that is, to lower the standard free energy of its predominant form. A consequence is that the change in free energy required for reduction of Zn(II) to Zn(Hg) is made larger. Since this added energy must be supplied electrically, the wave is displaced to more negative potentials (Figure 5.4.2). The stronger the binding in the complex (i.e., the larger K_c), the larger the shift from the free metal potential $E^{0'}_{M}$. Conveniently, K_c can be evaluated from this displacement:

$$E^{C}_{1/2} - E^{0'}_{M} = -\frac{RT}{nF} \ln K_c - \frac{RT}{nF} p \ln C^{*}_{X} + \frac{RT}{nF} \ln \frac{m_A}{m_C} \tag{5.4.81}$$

In a practice, $E^{0'}_{M}$ is usually identified with the voltammetric half-wave potential for the metal in a solution free of X, so that

$$E^{C}_{1/2} - E^{M}_{1/2} = -\frac{RT}{nF} \ln K_c - \frac{RT}{nF} p \ln C^{*}_{X} + \frac{RT}{nF} \ln \frac{m_M}{m_C} \tag{5.4.82}$$

From a plot of $E^{C}_{1/2}$ *vs.* $\ln C^{*}_{X}$ one can determine the stoichiometric number p. Equation 5.4.80 shows that such a plot should have a slope of $-pRT/nF$. Much that is known

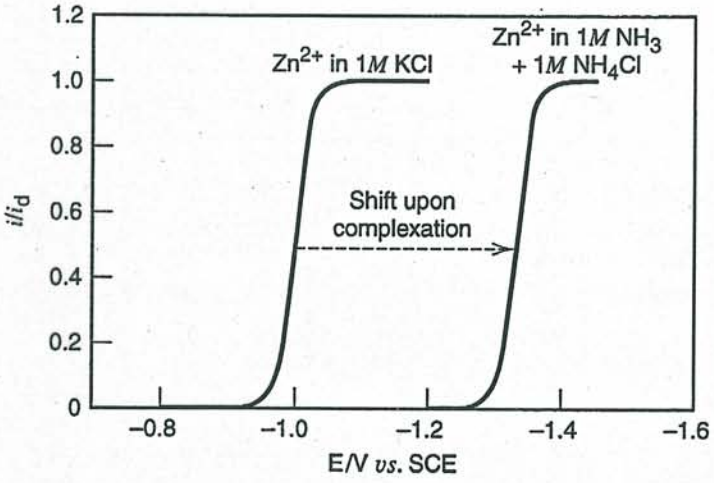

Figure 5.4.2 Shift of a reversible wave upon complexation of the reactant. Left curve is the reduction wave for Zn^{2+} in 1 *M* KCl at a Hg electrode ($E_{1/2} = -1.00$ V *vs.* SCE). Right curve is for Zn^{2+} in 1 *M* NH_3 + 1 *M* NH_4Cl ($E_{1/2} = -1.33$ V *vs.* SCE). Complexation by ammonia lowers the free energy of the oxidized form, so that it is no longer possible to reduce Zn(II) to the amalgam at the potentials of the wave recorded in the absence of ammonia. By applying a more negative potential, the combined free energy of Zn(II) plus the 2*e* on the electrode is elevated to match that of Zn(Hg) and interconversion between Zn(II) and Zn(Hg) becomes possible.

about the stoichiometry and stability constants of metal complexes has been determined from voltammetric measurements of the kind suggested here.

In the example just considered, the important feature was a shift in the wave position caused by selective chemical stabilization of one of the redox forms. In a reversible system the potential axis is a free energy axis, and the magnitude of the shift is a direct measure of the free energy involved in the stabilization. These concepts are quite general and can be used to understand many chemical effects on electrochemical responses. Any equilibrium in which either redox species participates will help to determine the wave position, and changes in concentrations of secondary participants in those equilibria (e.g., ammonia in the example above) will cause an additional shift in the half-wave potential. This state of affairs may seem confusing at first, but the principles are not complicated and are very valuable:

1. If the reduced form of a redox couple is chemically bound in an equilibrium process, then the reduced form has a lowered free energy relative to the situation where the binding is not present. Reduction of the oxidized form consequently becomes energetically easier, and oxidation of the reduced form becomes more difficult. Therefore, the voltammetric wave shifts in a positive direction by an amount reflecting the equilibrium constant (i.e., the change in standard free energy) for the binding process and the concentration of the binding agent.
2. If the oxidized form is chemically bound in an equilibrium process, then the oxidized form is stabilized. It becomes energetically easier to produce this species by oxidation of the reduced form, and it becomes harder to reduce the oxidized form. Accordingly, the voltammetric wave shifts in a negative direction by a degree that depends on the equilibrium constant for the binding process and the concentration of the binding agent. This is the situation that we encountered in the example involving $Zn(NH_3)_4^{2+}$ just above (Figure 5.4.2).
3. Increasing the concentration of the binding agent enlarges the equilibrium fraction of bound species, therefore the increase reinforces the basic effect and enhances the shift in the wave from its original position. We saw this feature in the example given above when we found that there is a progressive negative shift in the voltammetric wave for reduction of Zn(II) as the ammonia concentration is elevated.
4. Secondary equilibria can also affect the wave position in ways that can be interpreted within the framework of these first three principles. For example, the availability of ammonia in the buffer considered above is affected by the pH. If the pH were changed by adding HCl, the concentration of free ammonia would be lessened. Thus the added acid would tend to lower the fraction of complexation and would consequently cause a positive shift in the wave from its position before the change of pH, even though neither H^+ nor Cl^- is involved directly in the electrode process.
5. When both redox forms engage in binding equilibria, both are stabilized relative to the situation in which the binding processes are absent. The effects tend to offset each other. If the free energy of stabilization were exactly the same on both sides of the basic electron-transfer process, there would be no alteration of the free energy required for either oxidation or reduction, and the wave would not shift. If the stabilization of the oxidized form is greater, then the wave shifts in the negative direction, and vice versa.

A very wide variety of binding chemistry can be understood and analyzed within this framework. Obvious by the prior example is complexation of metals. Another case that we will soon encounter is the formation of metal amalgams, which produces useful positive shifts in waves for analytes of interest in polarography (Section 7.1.3). Generally important are acid-base equilibria, which affect many inorganic and organic redox species in protic media. The principles discussed here are also valid in systems involving such diverse phenomena as dimerization, ion pairing, adsorptive binding on a surface, coulombic binding to a polyelectrolyte, and binding to enzymes, antibodies, or DNA.

Detailed treatments like the one developed for the zinc–ammonia system are easily worked out for other types of electrode reactions, including

$$O + mH^+ + ne \rightleftarrows R + H_2O \qquad \text{(Problem 5.7)}$$
$$O + ne \rightleftarrows R(\text{adsorbed}) \qquad \text{(Chapter 14)}$$

Similar treatments can be developed for systems which do not involve the binding phenomena emphasized here, but which differ from the simple process $O + ne \rightleftarrows R$ and yet remain reversible. Such examples include

$$3O + ne \rightleftarrows R \qquad \text{(Problem 5.13)}$$
$$O + ne \rightleftarrows R(\text{insoluble}) \qquad \text{(Problem 5.5)}$$

Details are often available in references on polarography and voltammetry (28–30).

Reversible systems have the advantage of behaving as though all chemical participants are at equilibrium, thus they can be treated by any set of equilibrium relationships linking the species that define the oxidized and reduced states of the system. It is not important to treat the system according to an accurate mechanistic path, because the behavior is controlled entirely by free energy changes between initial and final states, and the mechanism is invisible to the experiment. In the case involving the zinc ammine complex discussed above, we formulated the chemistry as though the complex would become reduced by dissociating to produce Zn(II), which then would undergo conversion to the amalgam. This sequence probably does not describe the events in the real electrode process, but it offers a convenient thermodynamic cycle based on quantities that we can measure easily in other experiments, or perhaps even find in the literature.

In practical chemical analysis, one can obviously use half-wave potentials to identify the species giving rise to the observed waves; however the foregoing paragraphs illustrate the fact that the wave for a given species, such as Zn(II) can be found in different positions under different conditions. Thus it is important to control the analytical conditions, e.g. by employing a medium of controlled pH, buffer strength, and complexing characteristics. The analytical application of sampled current voltammetry is discussed more fully in Sections 7.1.3 and 7.3.6.

(d) Information from Change in Diffusion Current

For many processes D for MX_p is not very different from that of M, so that i_d, as given in (5.4.76) is about the same as that before complexation, as in the example in Figure 5.4.2. However if the ligand, X, is very large, as might occur when X is DNA, a protein, or a polymer, then the size of the species after complexation will be much larger than that of M, and there will be a significant decrease in D and in i_d. Under these conditions the change in i_d with addition of X can be used to obtain information about K_c and p. An investigation of this type was based on the interaction of $Co(phen)_3^{3+}$ with double-strand DNA (31), where phen is 1,10-phenanthroline. The diffusion coefficient decreased from 3.7×10^{-6} cm^2/s for the free Co species to 2.6×10^{-7} cm^2/s upon binding to DNA.

Sample calc^{n}s:

E	$i(\tau)$	$\ln\left(\frac{i_d - i}{i}\right)$
E_1	i_1	
E_2	i_2	
E_3	i_3	
E_4	i_4	
E_5	i_5	
⋮	⋮	⋮
	↑	
	identify i_d	

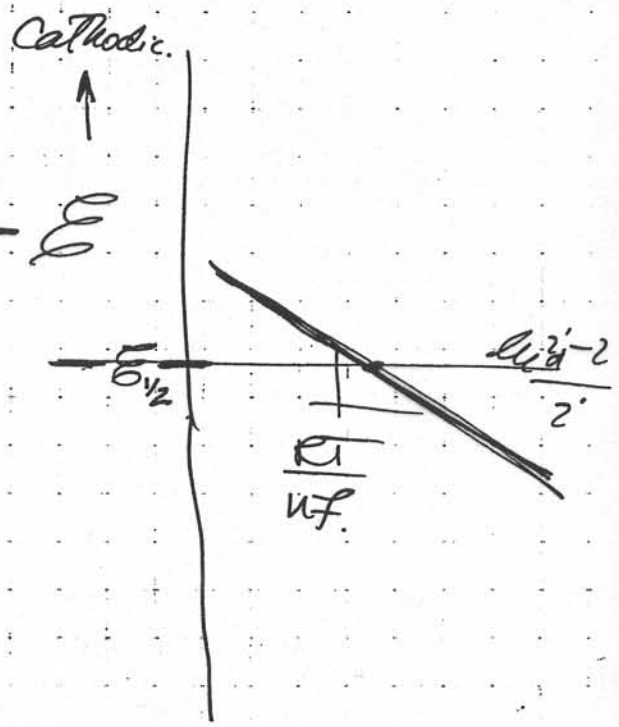

5.5 SAMPLED-CURRENT VOLTAMMETRY FOR QUASIREVERSIBLE AND IRREVERSIBLE ELECTRODE REACTIONS

In this section, we will treat the one-step, one-electron reaction $O + e \rightleftarrows R$ using the general (quasireversible) *i-E* characteristic. In contrast with the reversible cases just examined, the interfacial electron-transfer kinetics in the systems considered here are not so fast as to be transparent. Thus kinetic parameters such as k_f, k_b, k^0 and α influence the responses to potential steps and, as a consequence, can often be evaluated from those responses. The focus in this section is on ways to determine such kinetic information from step experiments, including sampled-current voltammetry. As in the treatment of reversible cases, the discussion will be developed first for early transients, then it will be redeveloped for the steady-state.

5.5.1 Responses Based on Linear Diffusion at a Planar Electrode

(a) Current-Time Behavior

The treatment of semi-infinite linear diffusion for the case where the current is governed by both mass transfer and charge-transfer kinetics begins according to the pattern used in Section 5.4.1. The diffusion equations for O and R are needed, as are the initial conditions, the semi-infinite conditions, and the flux balance. As we noted there, these lead to

$$\overline{C}_O(x, s) = \frac{C_O^*}{s} + A(s)e^{-(s/D_O)^{1/2}x} \tag{5.5.1}$$

$$\overline{C}_R(x, s) = -\xi A(s)e^{-(s/D_R)^{1/2}x} \tag{5.5.2}$$

where $\xi = (D_O/D_R)^{1/2}$.

For the quasireversible one-step, one-electron case, we can evaluate $A(s)$ by applying the condition:

$$\frac{i}{FA} = D_O\left(\frac{\partial C_O(x, t)}{\partial x}\right)_{x=0} = k_f C_O(0, t) - k_b C_R(0, t) \tag{5.5.3}$$

where

$$k_f = k^0 e^{-\alpha f(E-E^{0'})} \tag{5.5.4}$$

and

$$k_b = k^0 e^{(1-\alpha)f(E-E^{0'})} \tag{5.5.5}$$

with $f = F/RT$.

The transform of (5.5.3) is

$$D_O\left(\frac{\partial \overline{C}_O(x, s)}{\partial x}\right)_{x=0} = k_f \overline{C}_O(0, s) - k_b \overline{C}_R(0, s) \tag{5.5.6}$$

and, by substitution from (5.5.1) and (5.5.2),

$$A(s) = -\frac{k_f}{D_O^{1/2}} \frac{C_O^*}{s(H + s^{1/2})} \tag{5.5.7}$$

where

$$H = \frac{k_f}{D_O^{1/2}} + \frac{k_b}{D_R^{1/2}} \tag{5.5.8}$$

Then,

$$\bar{C}_O(x, s) = \frac{C_O^*}{s} - \frac{k_f C_O^* e^{-(s/D_O)^{1/2}x}}{D_O^{1/2} s(H + s^{1/2})} \tag{5.5.9}$$

From (5.5.3)

$$\bar{i}(s) = FAD_O\left[\frac{\partial \bar{C}_O(x, s)}{\partial x}\right]_{x=0} = \frac{FAk_f C_O^*}{s^{1/2}(H + s^{1/2})} \tag{5.5.10}$$

or, taking the inverse transform,

$$i(t) = FAk_f C_O^* \exp(H^2 t)\,\mathrm{erfc}(Ht^{1/2}) \tag{5.5.11}$$

For the case when R is initially present at C_R^*, equation 5.5.11 becomes

$$i(t) = FA(k_f C_O^* - k_b C_R^*) \exp(H^2 t)\,\mathrm{erfc}(Ht^{1/2}) \tag{5.5.12}$$

At a given step potential, k_f, k_b, and H are constants. The product $\exp(x^2)\mathrm{erfc}(x)$ is unity for $x = 0$, but falls monotonically toward zero as x becomes large; thus the current-time curve has the shape shown in Figure 5.5.1. Note that the kinetics limit the current at $t = 0$ to a finite value proportional to k_f (with R initially absent). In principle, k_f can be evaluated from the faradaic current at $t = 0$. Since a charging current also exists in the moments after the step is applied, the faradaic component at $t = 0$ typically would be determined by extrapolation from data taken after the charging current has decayed [see Sections 1.4.2 and 7.2.3(c)].

(b) Alternate Expression in Terms of η

If both O and R are present in the bulk, so that an equilibrium potential exists, one can describe the effect of potential on the current-time curve in terms of the overpotential, η. An alternate expression for (5.5.12) can be given by noting that

$$k_f C_O^* - k_b C_R^* = k^0 [C_O^* e^{-\alpha f(E-E^{0'})} - C_R^* e^{(1-\alpha)f(E-E^{0'})}] \tag{5.5.13}$$

or, by substituting for k^0 in terms of i_0 by (3.4.11),

$$k_f C_O^* - k_b C_R^* = \frac{i_0}{FA}[e^{-\alpha f\eta} - e^{(1-\alpha)f\eta}] \tag{5.5.14}$$

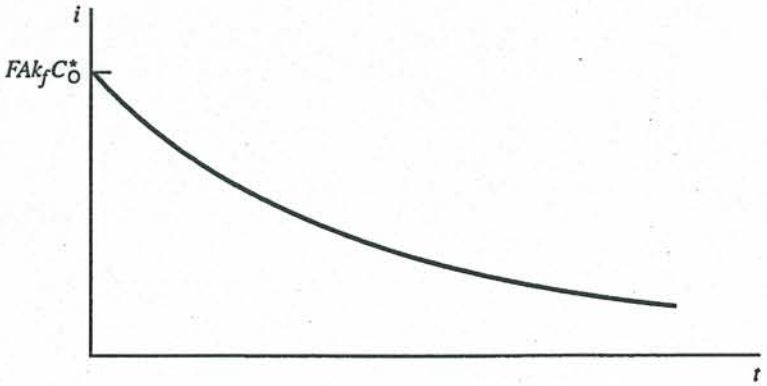

Figure 5.5.1 Current decay after the application of a step to a potential where species O is reduced with quasireversible kinetics.

Therefore, (5.5.12) may be written

$$i = i_0 [e^{-\alpha f\eta} - e^{(1-\alpha)f\eta}] \exp(H^2 t)\, \mathrm{erfc}(Ht^{1/2}) \tag{5.5.15}$$

By similar substitutions into the expression for H, one has

$$H = \frac{i_0}{FA}\left[\frac{e^{-\alpha f\eta}}{C_O^* D_O^{1/2}} - \frac{e^{(1-\alpha)f\eta}}{C_R^* D_R^{1/2}}\right] \tag{5.5.16}$$

Note that the form of (5.5.12) and (5.5.15) is

$$i = [i \text{ in the absence of mass-transfer effects}] \times [f(H, t)]$$

where $f(H, t)$ accounts for the effects of mass transfer.

(c) *Linearized Current-Time Curve*

For small values of $Ht^{1/2}$, the factor $\exp(H^2 t)\mathrm{erfc}(Ht^{1/2})$ can be linearized:

$$e^{x^2}\,\mathrm{erfc}(x) \simeq 1 - \frac{2x}{\pi^{1/2}} \tag{5.5.17}$$

Then, (5.5.11) becomes

$$i = FAk_f C_O^*\left(1 - \frac{2Ht^{1/2}}{\pi^{1/2}}\right) \tag{5.5.18}$$

In a system for which R is initially absent, one can apply a step to the potential region at the foot of the wave (where k_f, hence H, is still small), then plot i *vs.* $t^{1/2}$ and extrapolate the linear plot to $t = 0$ to obtain k_f from the intercept.

Likewise, (5.5.15) can be written

$$i = i_0 [e^{-\alpha f\eta} - e^{(1-\alpha)f\eta}]\left(1 - \frac{2Ht^{1/2}}{\pi^{1/2}}\right) \tag{5.5.19}$$

This relation applies only to a system containing both O and R initially, so that E_{eq} is defined. Stepping from E_{eq} to another potential involves a step of magnitude η; thus a plot of i *vs.* $t^{1/2}$ has as its intercept the kinetically controlled current free of mass-transfer effects. A plot of $i_{t=0}$ *vs.* η can then be used to obtain i_0.

For small values of η, the linearized i-η characteristic, (3.4.12), can be used, so that (5.5.15) becomes

$$i = -\frac{Fi_0\eta}{RT}\exp(H^2 t)\,\mathrm{erfc}(Ht^{1/2}) \tag{5.5.20}$$

Then for small η and small $Ht^{1/2}$ one has a "completely linearized" form:

$$i = -\frac{Fi_0\eta}{RT}\left(1 - \frac{2Ht^{1/2}}{\pi^{1/2}}\right) \tag{5.5.21}$$

(d) *Sampled-Current Voltammetry*

In preparation for deriving the shape of a sampled-current voltammogram, let us return to (5.5.11), which is the full current-time expression for the case where only species O is present in the bulk. Recognizing that $k_b/k_f = \theta = \exp[f(E - E^{0'})]$, we find that

$$H = \frac{k_f}{D_O^{1/2}}(1 + \xi\theta) \tag{5.5.22}$$

and that (5.5.11) can be rephrased as

$$i = \frac{FAD_O^{1/2}C_O^*}{\pi^{1/2}t^{1/2}(1 + \xi\theta)} [\pi^{1/2}Ht^{1/2} \exp(H^2t) \operatorname{erfc}(Ht^{1/2})] \tag{5.5.23}$$

Since semi-infinite linear diffusion applies, the diffusion-limited current is the Cottrell current, which is easily recognized in the factor preceding the brackets. Thus, we can simplify (5.5.23) to

$$i = \frac{i_d}{(1 + \xi\theta)} F_1(\lambda) \tag{5.5.24}$$

where

$$F_1(\lambda) = \pi^{1/2}\lambda \exp(\lambda^2)\operatorname{erfc}(\lambda) \tag{5.5.25}$$

and

$$\lambda = Ht^{1/2} = \frac{k_f t^{1/2}}{D_O^{1/2}}(1 + \xi\theta) \tag{5.5.26}$$

Equation 5.5.24 is a very compact representation of the way in which the current in a step experiment depends on potential and time, and it holds for all kinetic regimes: reversible, quasireversible, and totally irreversible. The function $F_1(\lambda)$ manifests the kinetic effects on the current in terms of the dimensionless parameter λ, which can be readily shown to compare the maximum current supportable by the reductive kinetic process at a given step potential ($FAk_fC_O^*$ *vs.* the maximum current supportable by diffusion at that potential [$i_d/(1+\xi\theta)$]. Thus a small value of λ implies a strong kinetic influence on the current, and a large value of λ corresponds to a situation where the kinetics are facile and the response is controlled by diffusion. The function $F_1(\lambda)$ rises monotonically from a value of zero at $\lambda = 0$ toward an asymptote of unity as λ becomes large (Figure 5.5.2).

Simpler forms of (5.5.24) are used for the reversible and totally irreversible limits. For example, consider (5.4.17), which we derived as a description of the current-time curve following an arbitrary step potential in a reversible system. That same relationship is available from (5.5.24) simply by recognizing that with reversible kinetics λ is very large, so that $F_1(\lambda)$ is always unity. The totally irreversible limit will be considered separately in Section 5.5.1(e).

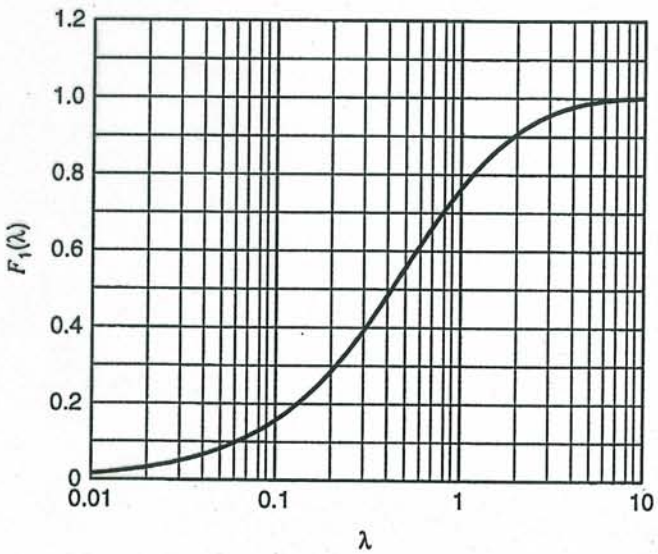

Figure 5.5.2 General kinetic function for chronoamperometry and sampled-current voltammetry.

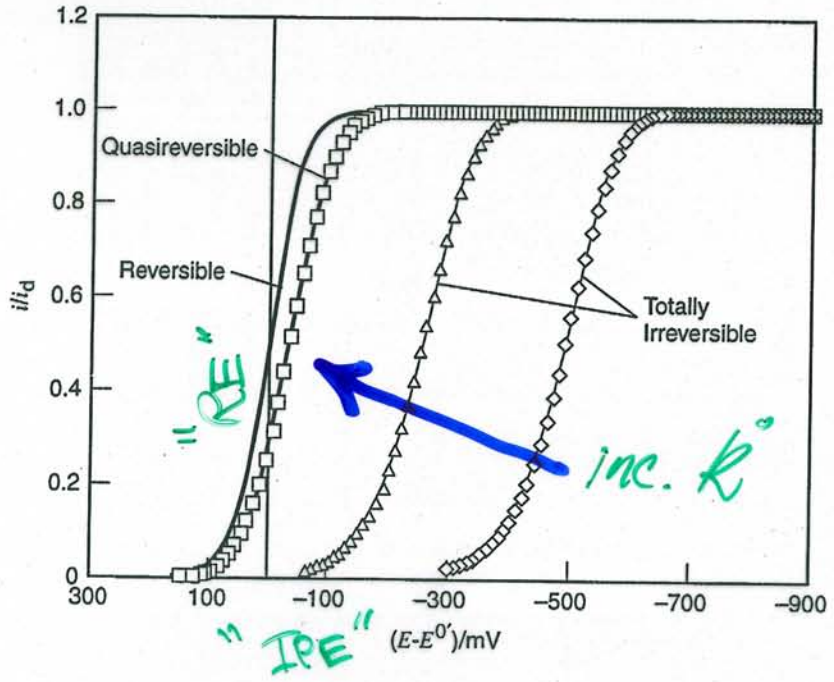

Figure 5.5.3 Sampled-current voltammograms for various kinetic regimes. Curves are calculated from (5.5.24) assuming Butler–Volmer kinetics with $\alpha = 0.5$ and $\tau = 1$ s, $D_O = D_R = 1 \times 10^{-5}$ cm^2/s. From left to right the values of k^0 are 10, 1×10^{-3}, 1×10^{-5}, and 1×10^{-7} cm/s.

So far, it has been most convenient to think of (5.2.24) as describing the current-time response following a potential step; however it also describes the current-potential curve in sampled-current voltammetry, just as we understood (5.4.17) to do for reversible systems. At a fixed sampling time τ, λ becomes $(k_f \tau^{1/2}/D_O^{1/2})(1 + \xi\theta)$, which is a function only of potential among the variables that change during a voltammetric run. At very positive potentials relative to $E^{0'}$, θ is very large, and $i = 0$. At very negative potentials, $\theta \to 0$ but k_f becomes very large; thus $F_1(\lambda)$ approaches unity, and $i \approx i_d$. From these simple considerations, we expect the sampled-current voltammogram to have a sigmoidal shape generally similar to that found in the reversible case. Figure 5.5.3, which contains several voltammograms corresponding to different kinetic regimes, bears out this expectation.

For very facile kinetics, corresponding to large k^0, the wave has the reversible shape, and the half-wave potential is near $E^{0'}$. (In Figure 5.5.3, where $D_O = D_R$, $E_{1/2} = E^{0'}$ exactly.) For smaller values of k^0, the kinetics must be driven, and the wave is displaced toward *more extreme* potentials (i.e., in the negative direction if the wave is for a reduction and in the positive direction for an oxidative wave). In addition, the wave is broadened by kinetic effects, as one can see clearly in Figure 5.5.3. The displacement is an overpotential and is proportional to the required kinetic activation. For small k^0, it can be hundreds of millivolts or even volts. Even so, k_f is activated exponentially with potential and can become large enough at sufficiently negative potentials to handle the diffusion-limited flux of electroactive species; thus the wave eventually shows a plateau at i_d, unless the background limit of the system is reached first.

(e) Totally Irreversible Reactions

The very displacement in potential that activates k_f also suppresses k_b; hence the backward component of the electrode reaction becomes progressively less important at potentials further to the negative side of $E^{0'}$. If k^0 is very small, a sizable activation of k_f is required for all points where appreciable current flows, and k_b is suppressed consistently to a negligible level. The irreversible regime is defined by the condition that $k_b/k_f \approx 0$ (i.e., $\theta \approx 0$) over the whole of the voltammetric wave. Then (5.5.11) becomes

$$i = FAk_f C_O^* \exp\left(\frac{k_f^2 t}{D_O}\right) \operatorname{erfc}\left(\frac{k_f t^{1/2}}{D_O^{1/2}}\right) \tag{5.5.27}$$

and (5.5.24) has the limiting form

$$\boxed{\frac{i}{i_d} = F_1(\lambda) = \pi^{1/2}\lambda \exp(\lambda^2)\,\mathrm{erfc}(\lambda)} \tag{5.5.28}$$

where λ has become $k_f t^{1/2}/{D_O}^{1/2}$.

The half-wave potential for an irreversible wave occurs where $F_1(\lambda) = 0.5$, which is where $\lambda = 0.433$. If k_f follows the usual exponential form and $t = \tau$, then

$$\frac{k^0\tau^{1/2}}{D_O^{1/2}} \exp\left[-\alpha f\left(E_{1/2} - E^{0'}\right)\right] = 0.433 \tag{5.5.29}$$

By taking logarithms and rearranging, one obtains

$$E_{1/2} = E^{0'} + \frac{RT}{\alpha F} \ln\left(\frac{2.31k^0\tau^{1/2}}{D_O^{1/2}}\right) \tag{5.5.30}$$

where the second term is the displacement required to activate the kinetics. Obviously (5.5.30) provides a simple way to evaluate k^0 if α is otherwise known.

(f) Kinetic Regimes

Conditions defining the three kinetic regimes can be distinguished in more precise terms by focusing on the particular value of λ at $E^{0'}$, which we will call λ^0. Since $k_f = k_b = k^0$ and $\theta = 1$ at $E^{0'}$, $\lambda^0 = (1 + \xi)k^0\tau^{1/2}/{D_O}^{1/2}$, which can be taken for our purpose as $2k^0\tau^{1/2}/{D_O}^{1/2}$. It is useful to understand λ^0 as a comparator of the intrinsic abilities of kinetics and diffusion to support a current. The greatest possible forward reaction rate at any potential is $k_f C_O^*$, corresponding to the absence of depletion at the electrode surface. At $E = E^{0'}$, this is $k^0 C_O^*$ and the resulting current is $FAk^0C_O^*$. The greatest current supportable by diffusion at sampling time τ is, of course, the Cottrell current. The ratio of the two currents is $\pi^{1/2}k^0\tau^{1/2}/D_O^{1/2}$, or $(\pi^{1/2}/2)\lambda^0$.

If a system is to appear reversible, λ^0 must be sufficiently large that $F_1(\lambda)$ is essentially unity at potentials neighboring $E^{0'}$. For $\lambda^0 > 2$ (or $k^0\tau^{1/2}/{D_O}^{1/2} > 1$), $F_1(\lambda^0)$ exceeds 0.90, a value high enough to assure reversible behavior within practical experimental limits. Smaller values of λ^0 will produce measurable kinetic effects in the voltammetry. Thus we can set $\lambda^0 = 2$ as the boundary between the reversible and quasireversible regimes, although we also recognize that the delineation is not sharp and that it depends operationally on the precision of experimental measurements.

Total irreversibility requires that $k_b/k_f \approx 0$ ($\theta \approx 0$) at all potentials where the current is measurably above the baseline. Because θ is also $\exp[f(E - E^{0'})]$, this condition simply implies that the rising portion of the wave be significantly displaced from $E^{0'}$ in the negative direction. If $E_{1/2} - E^{0'}$ is at least as negative as $-4.6RT/F$, then k_b/k_f will be no more than 0.01 at $E_{1/2}$, and the condition for total irreversibility will be satisfied. The implication is that the second term on the right side of (5.5.30) is more negative than $-4.6RT/nF$, and by rearrangement one finds that $\log\lambda^0 < -2\alpha + \log(2/2.31)$. The final term can be neglected for our purpose here, so the condition for total irreversibility becomes $\log\lambda^0 < -2\alpha$. For $\alpha = 0.5$, λ^0 must be less than 0.1.

In the middle ground, where $10^{-2\alpha} \leq \lambda^0 \leq 2$, the system is quasireversible, and one cannot simplify (5.5.24) as a descriptor of either current decay or voltammetric wave shape.

It is important to recognize that the kinetic regime, determined by λ^0, depends not only on the intrinsic kinetic characteristics of the electrode reaction, but also on the experimental conditions. The time scale, expressed as the sampling time τ in voltammetry, is a particularly important experimental variable and can be used to change the kinetic regime for a given system. For example, suppose one has an electrode reaction with the following (not unusual) properties: $k^0 = 10^{-2}$ cm/s, $\alpha = 0.5$, and $D_O = D_R = 10^{-5}$ cm^2/s. For

pling times longer than 1 s, $\lambda^0 > 2$ and the voltammetry would be reversible. Sampling times between 1 s and 250 μs correspond to $2 \geq \lambda^0 \geq 0.1$ and would produce quasireversible behavior. Values of τ smaller than 250 μs would produce total irreversibility.

5.5.2 General Current-Time Behavior at a Spherical Electrode

As a prelude to a treatment of steady-state voltammetry in quasireversible and totally irreversible systems, it is useful to develop a very general description of current flow in a step experiment at a spherical electrode. In Section 5.4.2(a) the basic diffusion problem was outlined, and the following relationships arose without invoking a particular kinetic condition.

$$\overline{C}_O(r, s) = \frac{C_O^*}{s} + \frac{A(s)}{r} e^{-(s/D_O)^{1/2} r} \tag{5.5.31}$$

$$\overline{C}_R(r, s) = -\frac{A(s)\xi^2\gamma}{r} e^{-(s/D_O)^{1/2} r_0} e^{-(s/D_R)^{1/2}(r - r_0)} \tag{5.5.32}$$

where $\xi = (D_O/D_R)^{1/2}$ and

$$\gamma = \frac{1 + r_0(s/D_O)^{1/2}}{1 + r_0(s/D_R)^{1/2}} \tag{5.5.33}$$

Now we are interested in determining the function $A(s)$ for a step experiment to an arbitrary potential, but where the electron-transfer kinetics are described explicitly in terms of k_f and k_b. By so doing, we will be able to use the results to define current-time responses for any sort of kinetic regime, whether reversible, quasireversible, or irreversible. The problem is developed just as in the sequence from (5.5.3) to (5.5.9), but in this instance, the results are

$$\overline{C}_O(r, s) = \frac{C_O^*}{s} - \frac{C_O^* r_0}{rs} \left[\frac{\dfrac{k_f r_0}{D_O}}{r_0 \left(\dfrac{s}{D_O} \right)^{1/2} + 1 + \dfrac{k_f r_0}{D_O} + \dfrac{k_b r_0 \xi^2 \gamma}{D_O}} \right] e^{-(s/D_O)^{1/2}(r - r_0)} \tag{5.5.34}$$

$$\overline{C}_R(r, s) = \frac{C_O^* r_0 \xi^2 \gamma}{rs} \left[\frac{\dfrac{k_f r_0}{D_O}}{r_0 \left(\dfrac{s}{D_O} \right)^{1/2} + 1 + \dfrac{k_f r_0}{D_O} + \dfrac{k_b r_0 \xi^2 \gamma}{D_O}} \right] e^{-(s/D_R)^{1/2}(r - r_0)} \tag{5.5.35}$$

As always, the current is proportional to the difference between the rates of the forward and backward reactions. In transform space,

$$\frac{\bar{i}(s)}{FA} = k_f \overline{C}_O(r_0, s) - k_b \overline{C}_R(r_0, s) \tag{5.5.36}$$

By substitution from (5.5.34) and (5.5.35) and algebraic rearrangement, one obtains the following general expression for the current transform:

$$\boxed{\bar{i}(s) = \frac{FAD_O C_O^*}{r_0 s} \left[\frac{\delta + 1}{\left(\dfrac{\delta + 1}{\kappa} \right) + (1 + \xi^2 \gamma \theta)} \right]} \tag{5.5.37}$$

sometimes provide approximate values of $E^{0'}$ in addition to kinetic parameters. Because the interpretation and information content of a wave's shape and position depends on the kinetic regime, it is essential to be able to diagnose the regime confidently.

Wave shape is a useful indicator toward that end, especially if the n-value is known. One can characterize reversibility either by the slope of a plot of E *vs.* $\log[(i_d - i)/i]$ (the "wave slope") or by the difference $|E_{3/4} - E_{1/4}|$ (the Tomeš criterion). Table 5.5.1 provides a summary of expectations for sampled-current voltammetry based either on early transients or on the steady state in all three kinetic regimes. For reversible systems, these figures of merit are near $60/n$ mV at ambient temperatures. Significantly larger figures often signal a degree of irreversibility. For example, if the one-step, one-electron mechanism applies and α is between 0.3 and 0.7 (commonly true), then a totally irreversible system would show $|E_{3/4} - E_{1/4}|$ between 65 and 150 mV. Except when α is toward the upper end of the range, such behavior would represent a clear departure from reversibility. Similar effects are seen in wave slopes; however it is not always easy to analyze them precisely, because wave-slope plots are slightly nonlinear for quasireversible voltammograms and for totally irreversible voltammograms based on early transients. The advantage of the Tomeš criterion is that it is always applicable.

If the electrode process is more complex than the one-step, one-electron model (e.g., $n > 1$ with a rate-determining heterogeneous electron transfer), then the wave shape can become extremely difficult to analyze. An exception is the case where the initial step is the rate-determining electron transfer [Section 3.5.4(b)], in which case all that has been discussed for totally irreversible systems also applies, but with the current multiplied consistently by n.

Although a large wave slope is a clear indicator that a system is not showing clean reversible behavior, it does not necessarily imply that one has an electrode process controlled by the kinetics of electron transfer. Electrode reactions frequently include purely chemical processes away from the electrode surface. A system involving "chemical complications" of this kind can show a wave shape essentially identical with that expected for a simple electron transfer in the totally irreversible regime. For example, the reduction of nitrobenzene in aqueous solutions can lead, depending on the pH, to phenylhydroxylamine (32):

$$PhNO_2 + 4H^+ + 4e \rightarrow \underset{\displaystyle H}{PhNOH} + H_2O \qquad (5.5.50)$$

However, the first electron-transfer step

$$PhNO_2 + e \rightarrow PhNO_2^{\cdot -} \qquad (5.5.51)$$

is intrinsically quite rapid, as found from measurements in nonaqueous solvents, such as DMF (32). The irreversibility observed in aqueous solutions arises because of the series of protonations and electron transfers following the first electron addition. If one

TABLE 5.5.1 Wave Shape Characteristics at 25°C in Sampled-Current Voltammetry

	Linear Diffusion		Steady State	
Kinetic Regime	Wave Slope/mV	$\lvert E_{3/4} - E_{1/4}\rvert$/mV	Wave Slope/mV	$\lvert E_{3/4} - E_{1/4}\rvert$/mV
Reversible ($n \geq 1$)	Linear, $59.1/n$	$56.4/n$	Linear, $59.1/n$	$56.4/n$
Quasireversible ($n = 1$)	Nonlinear	Between 56.4 and $45.0/\alpha$	Nonlinear	Between 56.4 and $56.4/\alpha$
Irreversible ($n = 1$)	Nonlinear	$45.0/\alpha$	Linear, $59.1/\alpha$	$56.4/\alpha$

If the voltammetry is quasireversible, one cannot use simplified descriptions of the wave shape, but must analyze results according to the appropriate general expression, either (5.5.24) or (5.5.44). The most useful approaches are:

1. *Method of Mirkin and Bard (33).* If the voltammetry is based on steady-state currents, one can analyze a quasireversible wave very conveniently in terms of two differences, $|E_{1/4} - E_{1/2}|$ and $|E_{3/4} - E_{1/2}|$. Mirkin and Bard have published tables correlating these differences with corresponding sets of k^0 and α; hence one can evaluate the kinetic parameters by a look-up process. Reference 33 contains a table for uniformly accessible electrodes, which applies to a spherical or hemispherical UME. A second table is given for voltammetry at a disk UME, which is not a uniformly accessible electrode.
2. *Curve fitting.* This method applies to voltammetry based on either transient or steady-state currents and proceeds essentially exactly as described for totally irreversible systems, except that the fitting function must be developed from (5.5.24) or (5.5.44).

For a quasireversible wave, $E_{1/2}$ is not far removed from $E^{0'}$ and is sometimes used as a rough estimate of the formal potential. Better estimates can be made from fundamental equations after the kinetic parameters have been evaluated from the wave shape. The tables published by Mirkin and Bard for their method actually provide $n(E_{1/2} - E^{0'})$ with sets of k^0 and α (33).

Whenever one is concerned with the evaluation of kinetic parameters, it is important to remember that the kinetic regime is defined partly by experimental conditions and that it can change if those conditions are altered. The most important experimental variable affecting the kinetic regime in voltammetry based on linear diffusion is the sampling time τ. For steady-state voltammetry, it is the radius of the electrode r_0. See Sections 5.5.1(f) and 5.5.3(b) for more detailed discussion. In estimating kinetic parameters, the actual shape of the electrode can be important. For example in making small electrodes (sub-μm radius), the metal disk is sometimes recessed inside the insulating sheath and has access to the solution only through a small aperture (Problem 5.17). Such an electrode will show a limiting current characteristic of the aperture radius, but the heterogeneous kinetics will be governed by the radius of the recessed disk (34, 35).

5.6 MULTICOMPONENT SYSTEMS AND MULTISTEP CHARGE TRANSFERS

Consider the case in which two reducible substances, O and O′, are present in the same solution, so that the consecutive electrode reactions $O + ne \rightarrow R$ and $O' + n'e \rightarrow R'$ can occur. Suppose the first process takes place at less extreme potentials than the second and that the second does not commence until the mass-transfer-limited region has been reached for the first. The reduction of species O can then be studied without interference from O′, but one must observe the current from O′ superimposed on that caused by the mass-transfer-limited flux of O. An example is the successive reduction of Cd(II) and Zn(II) in aqueous KCl, where Cd(II) is reduced with an $E_{1/2}$ near -0.6 V *vs.* SCE, but the Zn(II) remains inactive until the potential becomes more negative than about -0.9 V.

In the potential region where both processes are limited by the rates of mass transfer [i.e., $C_O(0, t) = C_{O'}(0, t) = 0$], the total current is simply the sum of the individual diffu-

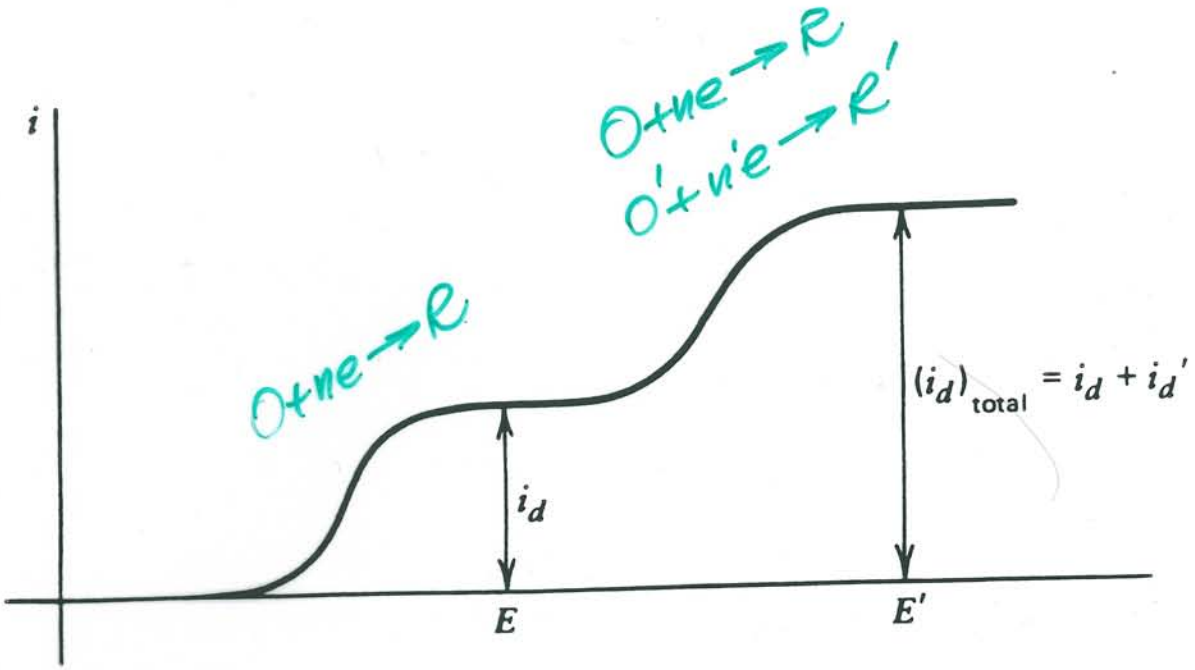

Figure 5.6.1

Sampled-current voltammogram for a two-component system.

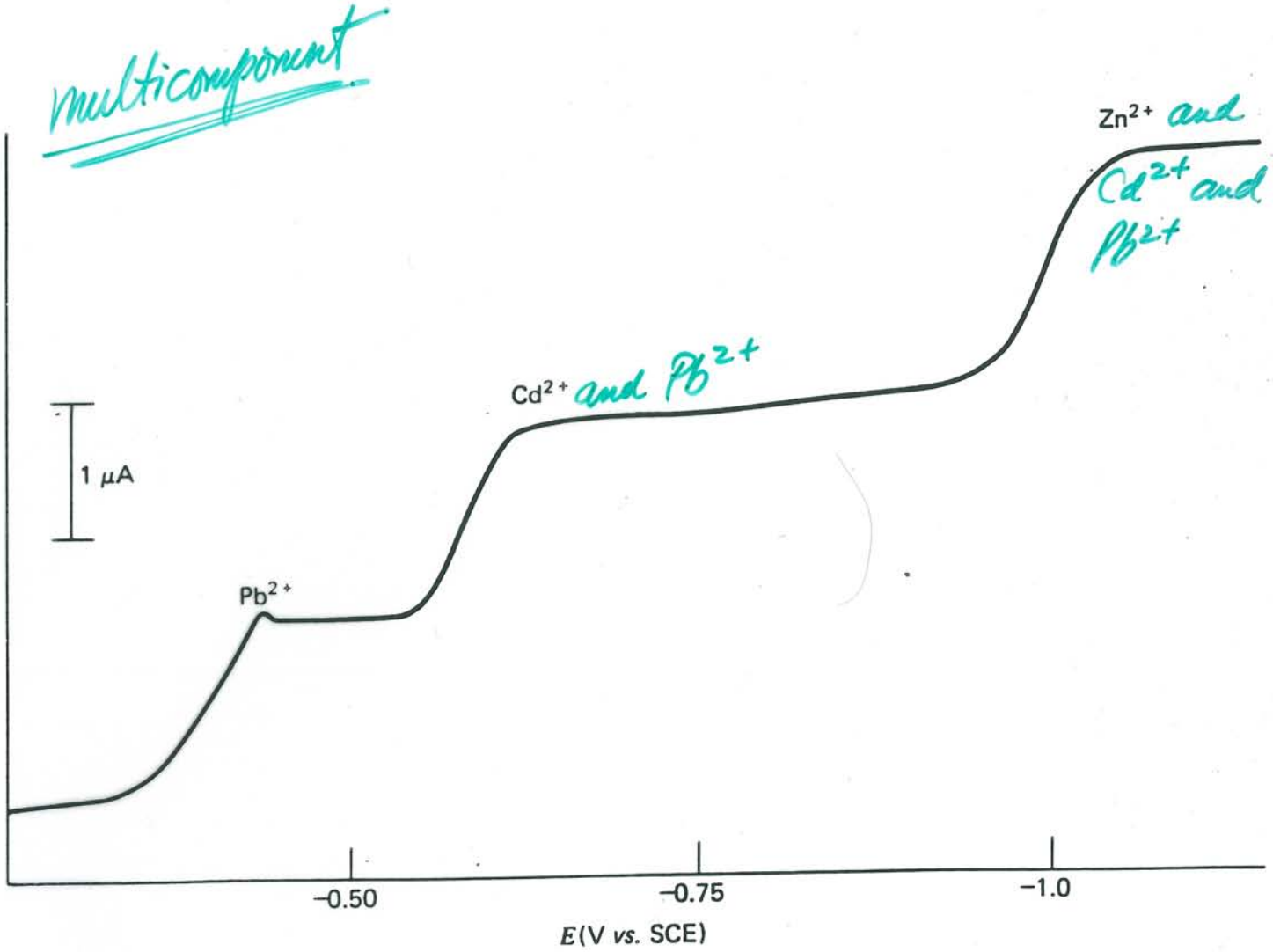

Figure 5.6.2

Polarogram of 0.2 m*M* Pb^{2+}, Cd^{2+}, and Zn^{2+} in 0.05 *M* KCl. The wave for Pb^{2+} shows a slight maximum of the type described in the note to Section 5.3.2. Only the envelope of the polarogram is shown here. Current oscillations are not depicted.

sion currents. For chronoamperometry or sampled-current voltammetry based on linear diffusion, one has

$$(i_d)_{\text{total}} = \frac{FA}{\pi^{1/2} t^{1/2}} (nD_O^{1/2} C_O^* + n' D_{O'}^{1/2} C_{O'}^*) \tag{5.6.1}$$

where t is either a sampling time or a variable time following the potential step. For sampled-current voltammetry based on the steady-state at an ultramicroelectrode

$$(i_d)_{\text{total}} = FA(nm_O C_O^* + n' m_{O'} C_{O'}^*) \tag{5.6.2}$$

where m_O and $m_{O'}$ are defined by Table 5.3.1 for the particular geometry of the UME.

In making measurements by sampled-current voltammetry, one would obtain traces like those in Figure 5.6.1. The diffusion current for the first wave can be subtracted from the total current of the composite wave to obtain the current attributable to O′ alone. That is,

$$i_d' = (i_d)_{\text{total}} - i_d \tag{5.6.3}$$

where i_d and i_d' are the current components due to O and O′, respectively.

This discussion assumes that the reactions of O and O′ are independent and that the products of one electrode reaction do not interfere with the other. While this is frequently the situation, there are cases where reactions in solution can perturb the diffusion currents and invalidate (5.6.3) (36). The classic case is the reduction of cadmium ion and iodate at a mercury electrode in an unbuffered medium, where O is Cd^{2+} and O′ is IO_3^-. The reduction of IO_3^- in the second wave occurs by the reaction $IO_3^- + 3H_2O + 6e \rightarrow I^- + 6OH^-$. The liberated hydroxide diffuses away from the electrode and reacts with Cd^{2+} diffusing toward the electrode, causing precipitation of $Cd(OH)_2$ and thus decreasing the contribution of the first wave (from reduction of Cd^{2+} to the amalgam) at potentials where the second wave occurs. The consequence is a second plateau that is much lower than that observed if the reactions were independent (or if the solution were buffered).

Similar considerations hold for a system in which a single species O is reduced in several steps, depending on potential, to more than one product. That is,

$$O + n_1 e \rightarrow R_1 \tag{5.6.4}$$

$$R_1 + n_2 e \rightarrow R_2 \tag{5.6.5}$$

where the second step occurs at more extreme potentials than the first. A simple example is molecular oxygen, which is reduced in two steps in neutral solution. Figure 5.6.2 shows the behavior of this system in the polarographic form of sampled-current voltammetry. (See Chapter 7 for more on polarography.) In the first reduction step, oxygen goes to hydrogen peroxide with a two-electron change manifested by a wave near −0.1 V *vs.* SCE.

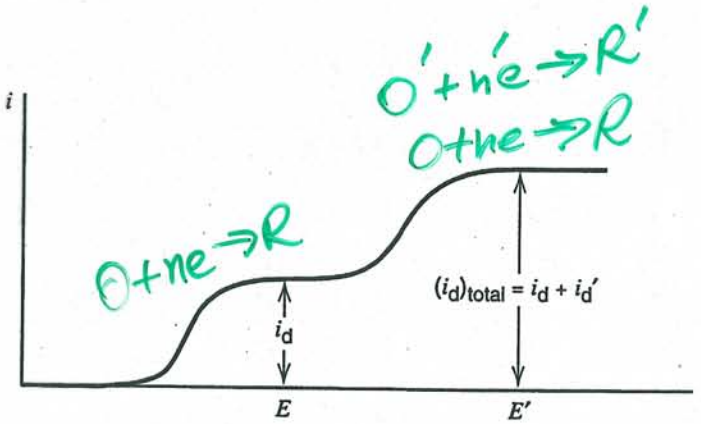

Figure 5.6.1 Sampled-current voltammogram for a two-component system.

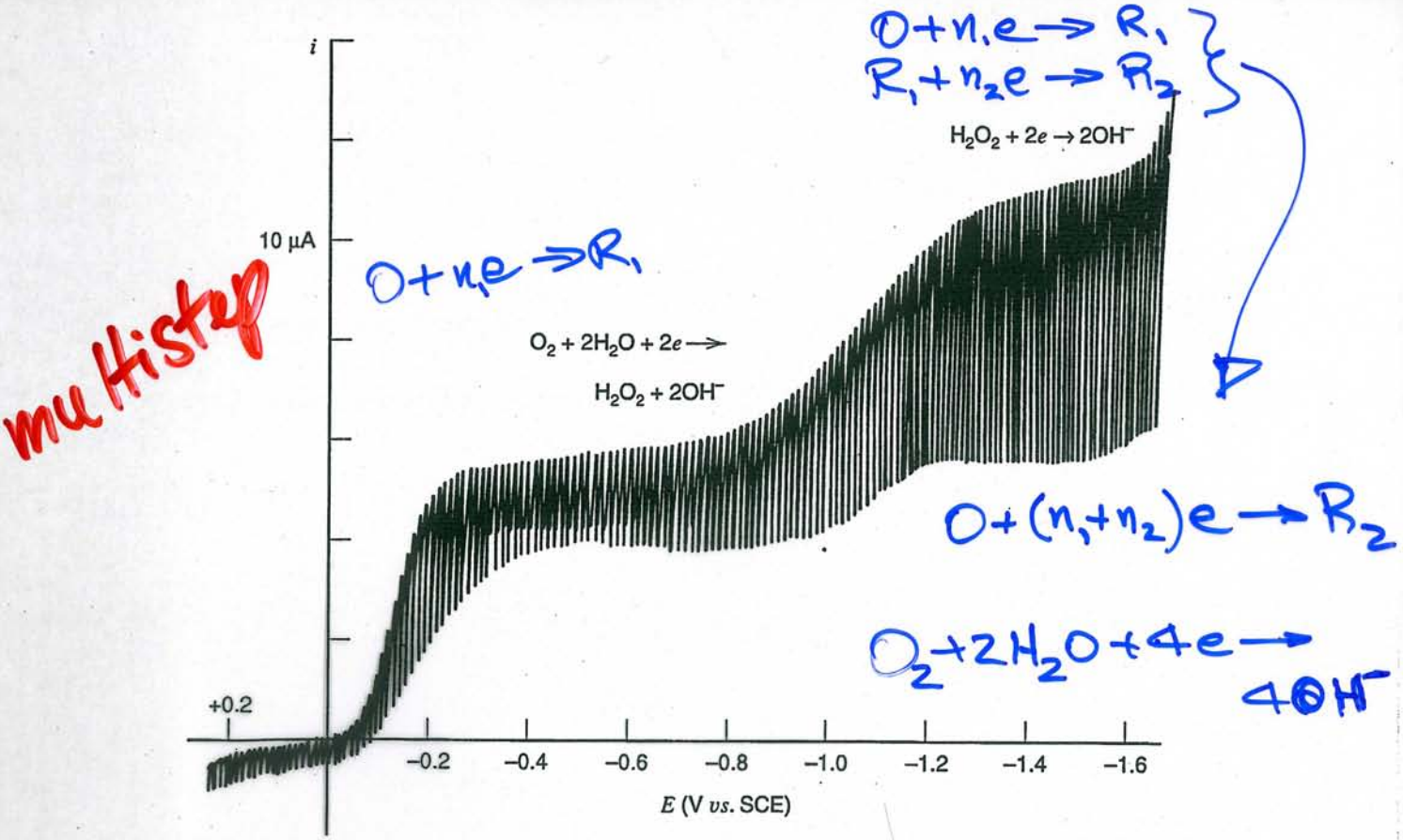

Figure 5.6.2 Polarographic form of sampled-current voltammetry for air-saturated 0.1 *M* KNO_3 with Triton X-100 added as a maximum suppressor. The working electrode is a dropping mercury electrode, which produces oscillations as individual drops grow and fall. This curve was recorded in the classical mode using a recorder that was fast enough to follow current changes near the end of drop life, but not at drop fall, when the current goes almost to zero. The top edge of the envelope can be regarded as a sampled-current voltammogram.

A second two-electron step takes hydrogen peroxide to water. At potentials less extreme than about −0.5 V, the second step does not occur to any appreciable extent; hence one sees only a single wave corresponding to a diffusion-limited, two-electron process. At still more negative potentials, the second step begins to occur, and beyond −1.2 V oxygen is reduced completely to water at the diffusion-limited rate.

For the entire process [(5.6.4) and (5.6.5)], it is clear that at potentials for which the reduction of O to R_2 is diffusion controlled, the early transient current following a potential step is simply

$$i_d = \frac{FAD_O^{1/2}C_O^*}{\pi^{1/2}t^{1/2}}(n_1 + n_2) \tag{5.6.6}$$

and the steady-state current at a UME is

$$i_d = FAm_O C_O^*(n_1 + n_2) \tag{5.6.7}$$

where m_O is given for the particular geometry in Table 5.3.1. Equations for currents measured in sampled-current voltammetric experiments can be written analogously. Our focus here is on the limiting current resulting from a multistep electron transfer involving a given chemical species. There are, in addition, many interesting kinetic and mechanistic aspects to processes involving sequential electron transfers, but we defer them for consideration in Chapter 12.

Reduction of Oxygen:

$$O_2 + 2H_2O + 4e \rightarrow 4OH^-$$

Oxidation of hydrogen:

$$2H_2 \rightarrow 4H^+ + 4e$$

Overall cell reaction:

$$2H_2 + O_2 + 2H_2O \rightarrow 4H^+ + 4OH^-$$

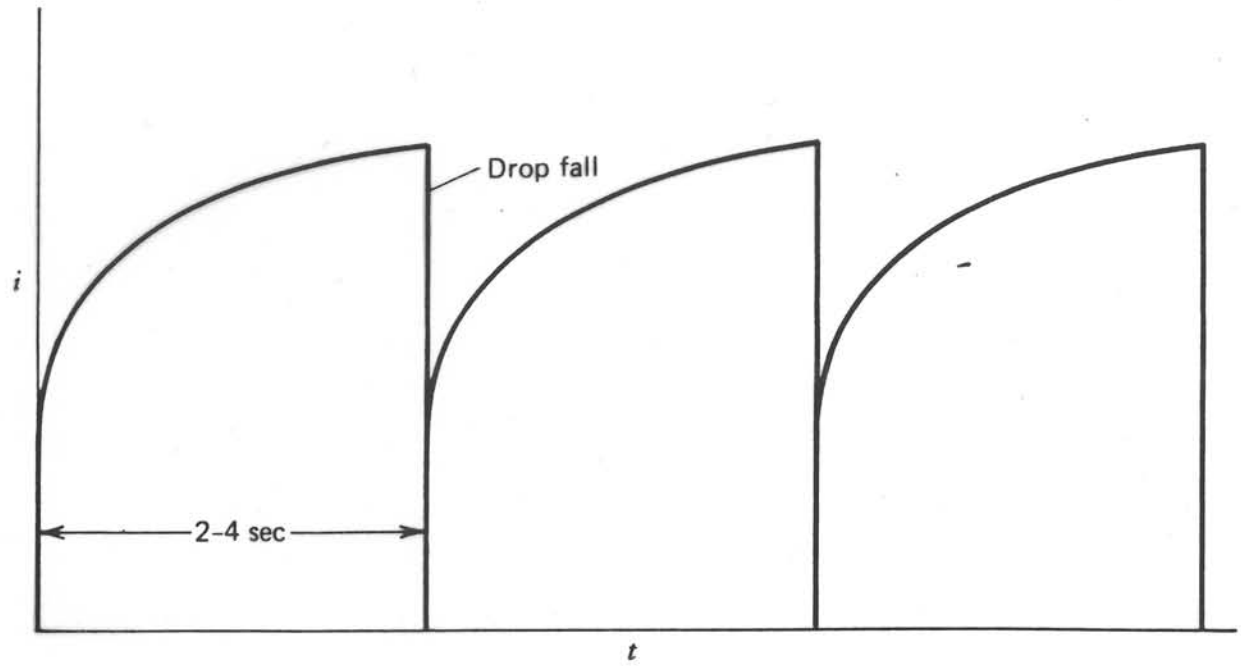

Figure 5.3.2
Current growth during three successive drops of a DME.

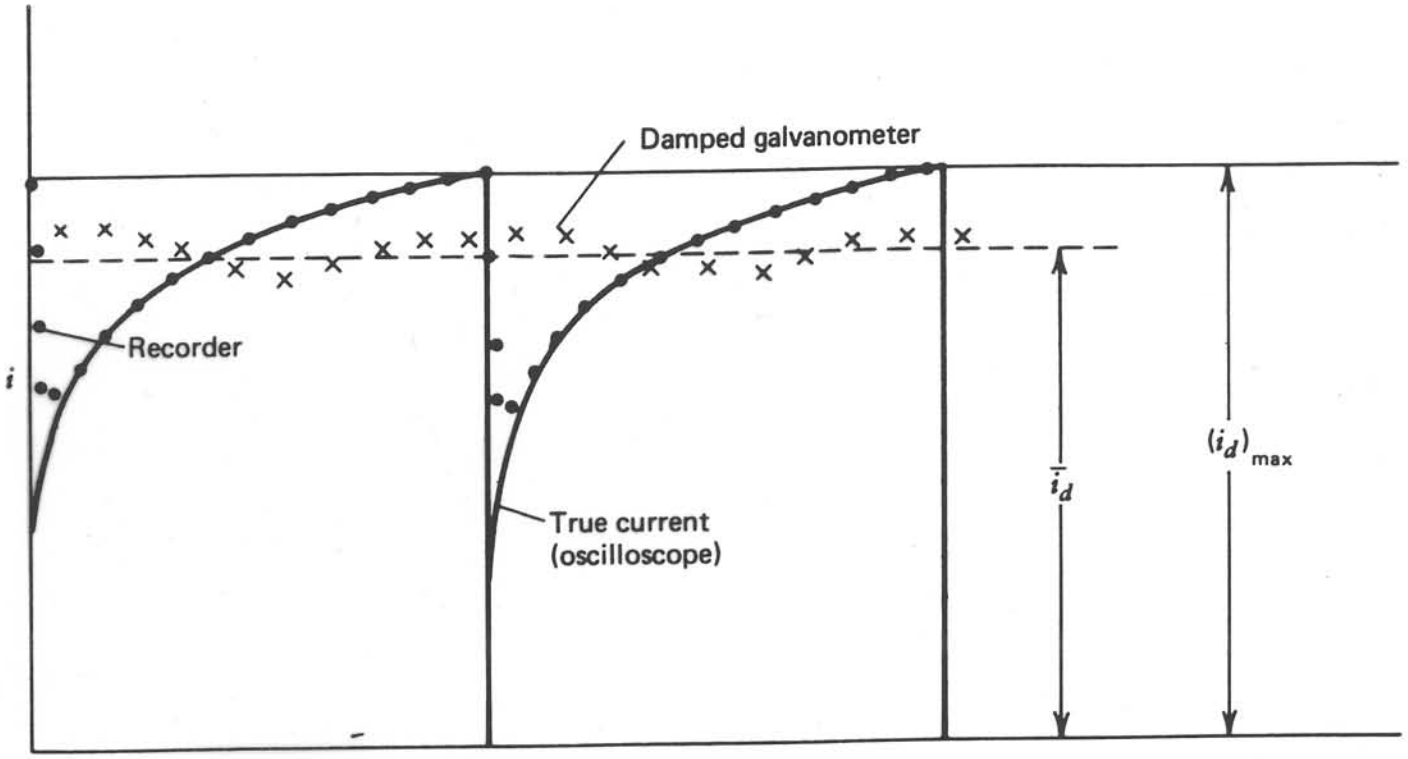

Figure 5.3.4

Current-time curves during individual drops at a DME as observed with three different recording devices.

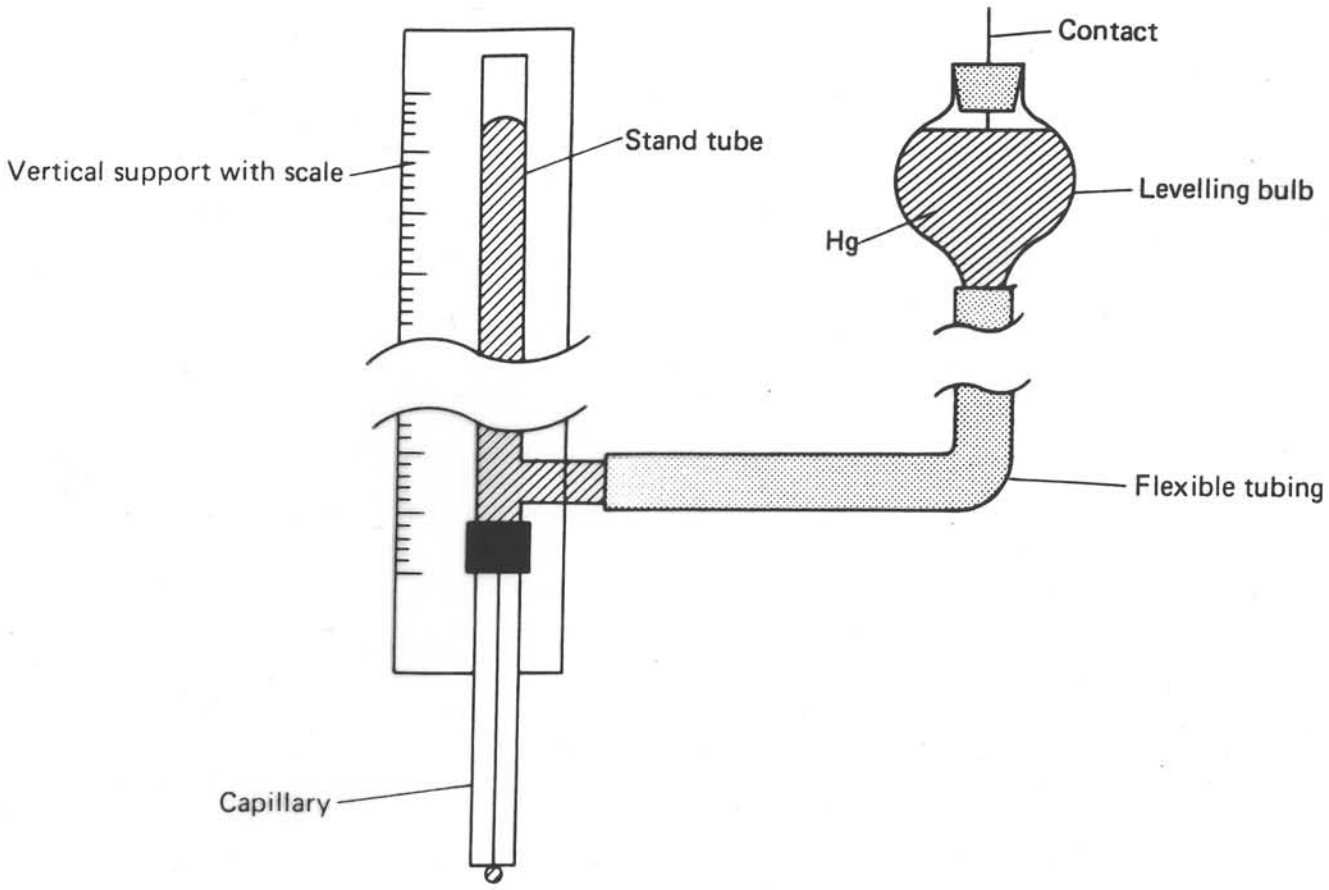

Figure 5.3.1
A dropping mercury electrode.

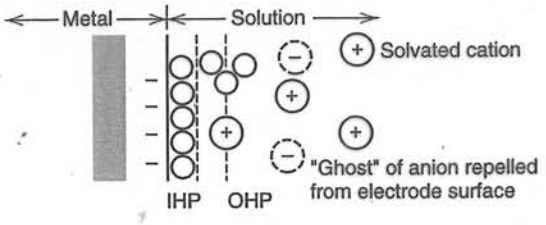

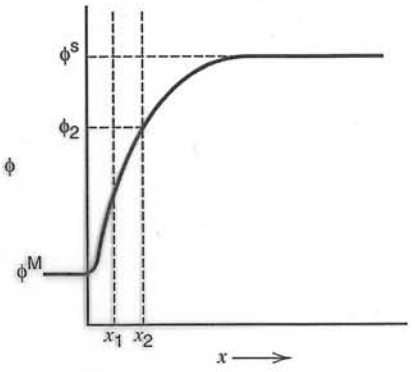

Figure 1.2.4 Potential profile across the double-layer region in the absence of specific adsorption of ions. The variable ϕ, called the *inner potential*, is discussed in detail in Section 2.2. A more quantitative representation of this profile is shown in Figure 12.3.6.

1.2.4 Double-Layer Capacitance and Charging Current in Electrochemical Measurements

Consider a cell consisting of an IPE and an ideal reversible electrode. We can approximate such a system with a mercury electrode in a potassium chloride solution that is also in contact with an SCE. This cell, represented by Hg/K^+, Cl^-/SCE, can be approximated by an electrical circuit with a resistor, R_s, representing the solution resistance and a capacitor, C_d, representing the double layer at the $Hg/K^+,Cl^-$ interface (Figure 1.2.5).[5] Since

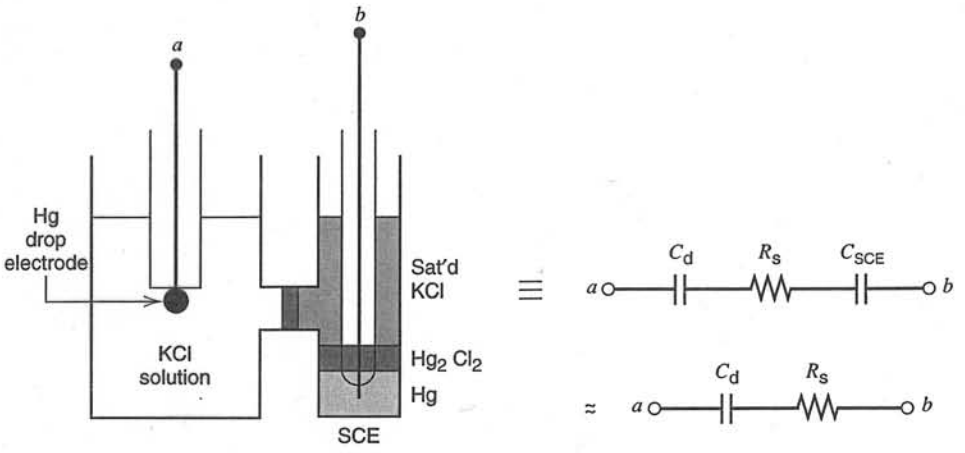

Figure 1.2.5 *Left*: Two-electrode cell with an ideal polarized mercury drop electrode and an SCE. *Right*: Representation of the cell in terms of linear circuit elements.

[5]Actually, the capacitance of the SCE, C_{SCE}, should also be included. However, the series capacitance of C_d and C_{SCE} is $C_T = C_d C_{SCE}/[C_d + C_{SCE}]$, and normally $C_{SCE} >> C_d$, so that $C_T \approx C_d$. Thus, C_{SCE} can be neglected in the circuit.

C_d is generally a function of potential, the proposed model in terms of circuit elements is strictly accurate only for experiments where the overall cell potential does not change very much. Where it does, approximate results can be obtained using an "average" C_d over the potential range.

Information about an electrochemical system is often gained by applying an electrical perturbation to the system and observing the resulting changes in the characteristics of the system. In later sections of this chapter and later chapters of this book, we will encounter such experiments over and over. It is worthwhile now to consider the response of the IPE system, represented by the circuit elements R_s and C_d in series, to several common electrical perturbations.

(a) Voltage (or Potential) Step

The result of a potential step to the IPE is the familiar *RC* circuit problem (Figure 1.2.6). The behavior of the current, i, with time, t, when applying a potential step of magnitude E, is

$$\boxed{i = \frac{E}{R_s} e^{-t/R_s C_d}} \tag{1.2.6}$$

This equation is derived from the general equation for the charge, q, on a capacitor as a function of the voltage across it, E_C:

$$q = C_d E_C \tag{1.2.7}$$

At any time the sum of the voltages, E_R and E_C, across the resistor and the capacitor, respectively, must equal the applied voltage; hence

$$E = E_R + E_C = iR_s + \frac{q}{C_d} \tag{1.2.8}$$

Noting that $i = dq/dt$ and rearranging yields

$$\frac{dq}{dt} = \frac{-q}{R_s C_d} + \frac{E}{R_s} \tag{1.2.9}$$

If we assume that the capacitor is initially uncharged ($q = 0$ at $t = 0$), then the solution of (1.2.9) is

$$q = EC_d[1 - e^{-t/R_s C_d}] \tag{1.2.10}$$

By differentiating (1.2.10), one obtains (1.2.6). Hence, for a potential step input, there is an exponentially decaying current having a time constant, $\tau = R_s C_d$ (Figure 1.2.7). The current for charging the double-layer capacitance drops to 37% of its initial value at $t = \tau$, and to 5% of its initial value at $t = 3\tau$. For example, if $R_s = 1\ \Omega$ and $C_d = 20\ \mu$F, then $\tau = 20\ \mu$s and double-layer charging is 95% complete in 60 μs.

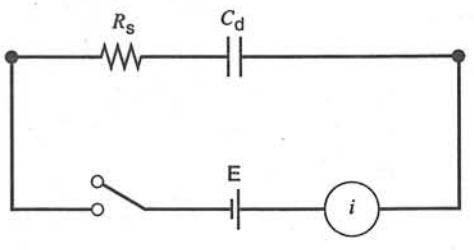

Figure 1.2.6 Potential step experiment for an *RC* circuit.

The point is that if we take a system that is reasonably fast and set τ too low, we can make the system appear

Quasi reversible

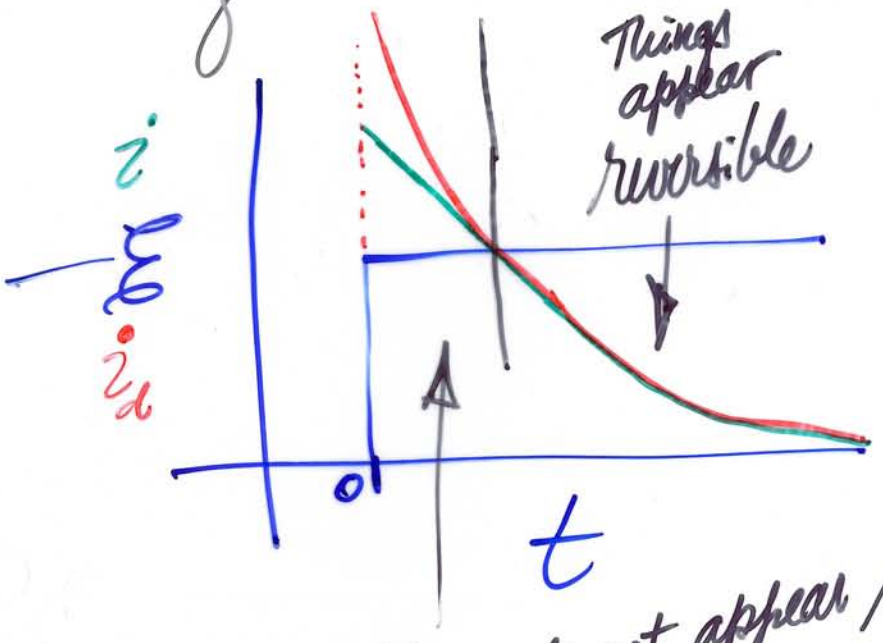

Things do not appear reversible

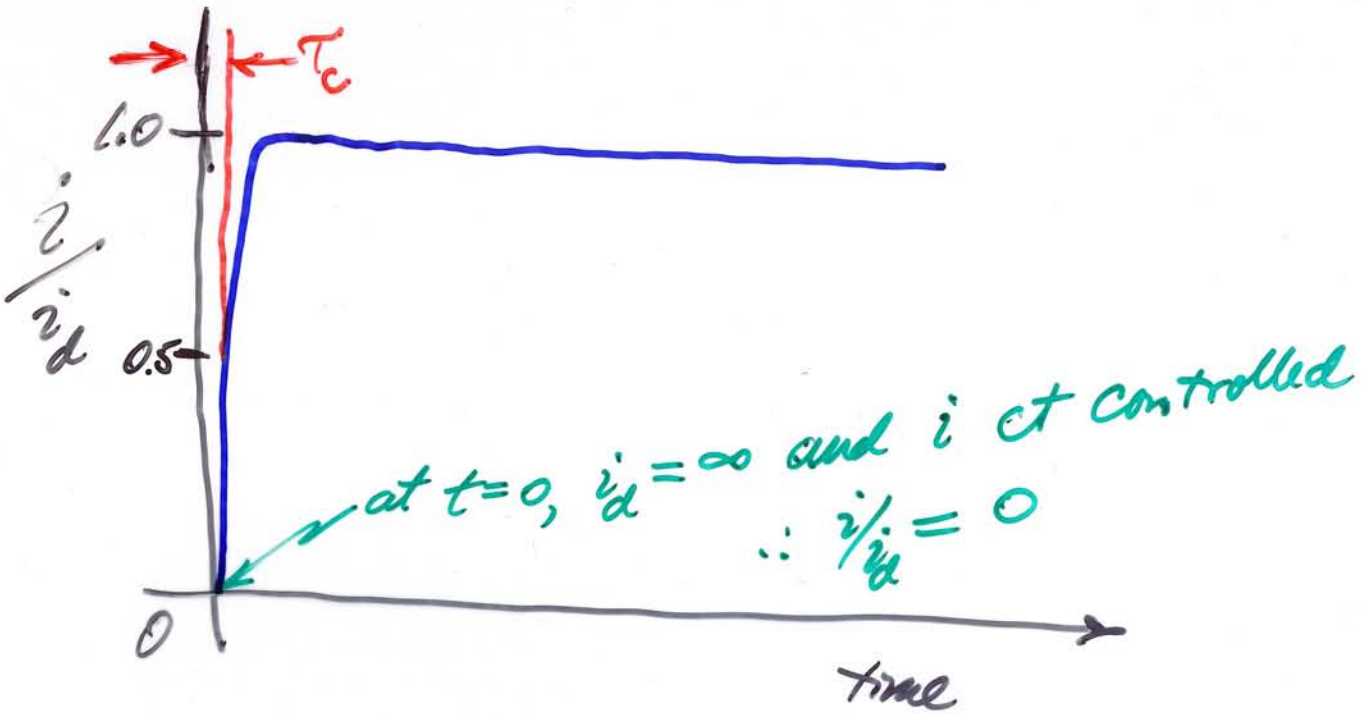

when $\frac{i}{i_d} = \frac{1}{2} = \pi^{1/2} \lambda \exp \lambda^2 \operatorname{erfc} \lambda$

$\log \lambda = -0.348 \Rightarrow \lambda = 0.449 = \frac{k_f \tau^{1/2}}{D_0^{1/2}}$

$\therefore$ critical time, τ_c, is given by

$$\tau_c = \frac{(0.202) D_0}{k_f^2}$$, i.e., at this time, $i/i_d = 0.5$

Choose $D_0 = 5 \times 10^{-5}$ cm^2/s — what happens when

$k_f = 10^{-1}$ cm/s ? $\tau_c = 1$ ms

$k_f = 10$ cm/s ? $\tau_c = 0.1$ μs

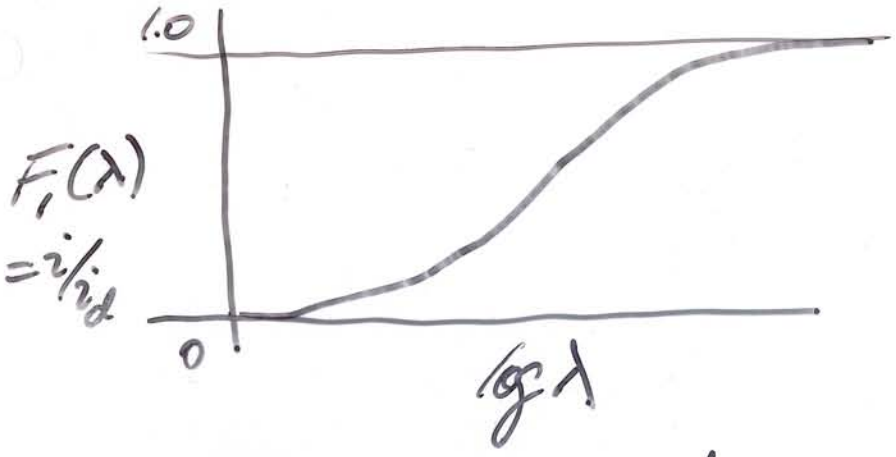

$$A = \frac{k_f t^{1/2}}{D_0^{1/2}}$$

Recall that $\lambda \propto k_f t^{1/2}$ or $k_f \tau^{1/2}$

↑ Polarography ↑ planar μelectrode voltammetry

Suppose $\tau = 1s$

sufficiently cathodic to allow us to neglect the back rxn.

System will appear reversible ⇒ not control.